Generating spatially separated correlated multiphoton states in nonlinear waveguide quantum electrodynamics

Jia-Qi Li, Anton Frisk Kockum, and Xin Wang^{1,*}

¹Shaanxi Province Key Laboratory of Quantum Information and Quantum Optoelectronic Devices, School of Physics, Xi'an Jiaotong University, Xi'an 710049, People's Republic of China ²Department of Microtechnology and Nanoscience, Chalmers University of Technology, 41296 Gothenburg, Sweden (Dated: November 19, 2025)

Strongly correlated multi-photon states are indispensable resources for advanced quantum technologies, yet their deterministic generation remains challenging due to the inherent weak nonlinearity in most optical systems. Here, we propose a scalable architecture for producing correlated fewphoton entangled states via cascaded inelastic scattering in a nonlinear waveguide. When a single photon scatters off a far detuned excited two-level emitter, it coherently converts into a propagating doublon, a bound photon pair with anomalous dispersion. This doublon can subsequently scatter off a downstream excited emitter to further convert into a triplon, and so on, thereby establishing a photon-number amplification cascade $|\cdot\rangle\rightarrow|:\rangle\rightarrow|:\rangle\rightarrow.$ Central to this process is the concept of a pseudo-giant atom, which we introduce here to capture the non-local scattering potential emergent from the wave functions of bound states. By implementing this scheme using a real giant atom with multiple engineered coupling points, we achieve unidirectional and full controllable photon conversion without backscattering. The resulting output state forms a programmable superposition of spatially and temporally isolated photon-number components, automatically sorted by their distinct group velocities. This work opens a new paradigm in quantum state engineering, enabling on-demand generation of complex multi-photon resources for quantum simulation, metrology, and scalable quantum networks.

I. INTRODUCTION

Strongly correlated multi-photon states are fundamental to modern quantum technologies, enabling quantumenhanced metrology, scalable quantum networks, and quantum simulation of many-body physics [1–3]. However, generating such states often requires strong optical nonlinearities at the few-photon level, which remains a significant challenge due to the inherently weak photonphoton interactions [4]. Conventional approaches for generating multi-photon states in waveguide quantum electrodynamics (wQED) leverage two-level emitters (TLEs) as nonlinear impurities with infinite on-site interaction $(U \to \infty)$, but the limited optical depth constrains the efficiency of the multi-photon state generation [5–7]. Alternative strategies employing extended emitter ensembles [8–10] or strong coupling [11–13] face challenges in accuracy, control, and scalability.

Another alternative route to generation of multiphoton states is nonlinear photonic baths. Here, the nonlinearity is directly embedded into the bath, described by a Kerr-type or Bose–Hubbard Hamiltonian. In such systems, photons directly experience pairwise interactions, leading to the formation of multi-photon bound states [14]. In experimental platforms for quantum simulation [15], such Hamiltonians arise naturally, e.g., from the intrinsic anharmonicity of the transmon qubit in circuit QED [16–21] and the dipole blockade in Rydberg atom arrays [22–24]. Crucially, these multi-photon

bound states, such as doublons (two-photon states) and triplons (three-photon states), inherit dispersion relations different from the linear multi-photon scattering state, behaving as quasi-particles with defined velocity and energy [25–27]. However, dynamically generating, manipulating, and spatially isolating these complex states within a single platform remains elusive.

Here, we introduce a cascaded inelastic scattering process within a nonlinear waveguide that overcomes these limitations. Our approach exploits far detuned excited TLEs as non-resonant mediators, enabling a controlled sequential upconversion of photon-number correlations [see Fig. 1(a)]. Crucially, an incident single photon (S)scatters off the first excited TLE to deterministically generate a propagating doublon (D), a bound photon pair with unique dispersion. This doublon state then acts as the input for a second scattering event off a subsequent excited TLE, coherently upconverting it into a triplon (T), and so forth for higher-order states. Compared to the conventional point-like TLE scattering potential, a distinguishing feature of the process here is that central to it is the formation of an effective non-local scattering potential mediated by the propagating bound states themselves. Inspired by giant atoms [28–32], emitters coupled to a waveguide a multiple separate points, we formalize the concept of this nonlocal scattering potential as a pseudo-giant atom (PGA).

By utilizing real giant atoms (RGAs) with engineered coupling strengths and phases at multiple points in the waveguide, our cascaded architecture turns out to allow tuning of the $S \to D \to T$ conversion efficiency across nearly the full range. Furthermore, the scattering pro-

^{*} wangxin.phy@xjtu.edu.cn

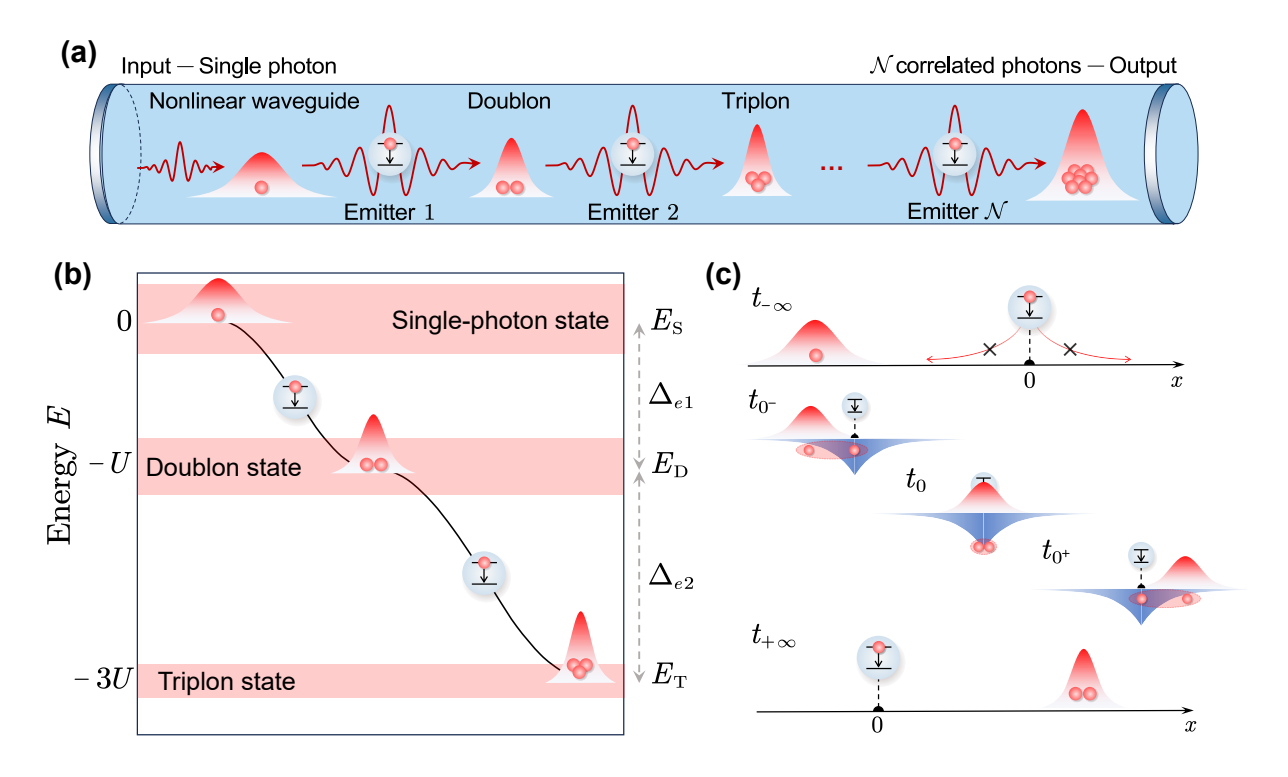


FIG. 1. Schematic of cascaded scattering in a nonlinear waveguide. (a) A single photon incident from the left in the waveguide first scatters off a detuned excited emitter, generating a pair of correlated photons—a doublon. The doublon subsequently scatters off a second excited emitter, producing three correlated photons—a triplon. This cascaded scattering process can, in principle, be extended to generate \mathcal{N} correlated photons. (b) Energy-level structure for single- $(E_{\rm S})$, two- $(E_{\rm D})$, and three-photon $(E_{\rm T})$ wave packets and the emitters with transition frequencies detuned by Δ_{e1} and Δ_{e2} from the waveguide cavity frequency ω_c . The bandwidth of the single-photon band is 4J; the doublon and triplon bands are more narrow than that, and are not shown exactly to scale in this illustration. (c) Temporal evolution of the scattering process. The shading depth at times $\{t_{0-}, t_0, t_{0+}\}$ represents the instantaneous effective scattering strength.

cess exhibits remarkable unidirectionality rooted in quantum interference. Specifically, when the coupling parameters are tuned well, the single-photon (doublon) undergoes almost complete chiral conversion into a forward-propagating doublon (triplon), without residual single-photon transmission or reflection. The precise interference control within the giant atom's coupling profile enables an almost perfect cascaded flow of quantum states without backscattering losses, accompanied by sequentially increasing photon-number correlations.

Another defining feature of our platform is the automatic spatiotemporal sorting of the generated quantum state. Owing to the intrinsic photon-number-dependent group velocities $(v_g^{(1)} > v_g^{(2)} > v_g^{(3)})$ inherent to the distinct dispersion relations of the multi-photon state, the output wavepacket naturally separates into distinct spatially ordered temporal bins. The resulting output state is a programmable superposition of spatially isolated correlated quantum states:

$$|\Psi_{\text{out}}\rangle = \alpha |S\rangle_{\tau_1} + \beta |D\rangle_{\tau_2} + \gamma |T\rangle_{\tau_3},$$
 (1)

where $\tau_1 < \tau_2 < \tau_3$ mark the arrival times of the singlephoton, doublon, and triplon components, respectively, with the tunable conversion efficiencies $\alpha, \beta, \gamma \in [0, 1)$

fulfilling
$$|\alpha|^2 + |\beta|^2 + |\gamma|^2 = 1$$
.

This work establishes cascaded inelastic scattering in nonlinear waveguides as a powerful paradigm for quantum state engineering. Unlike existing approaches [33, 34], our architecture requires only a single TLE per scattering stage, thereby reducing system complexity while enhancing scalability and flexibility. The PGA framework extends scattering theory into the nonlinear waveguide regime by revealing how bound states generate emergent non-local scattering potentials. The combination of cascaded generation, programmable entanglement manipulation, and automatic spatiotemporal sorting of multi-photon states opens new possibilities for complex quantum many-body state synthesis, resource-efficient photonic quantum computing, and quantum networks requiring distributed entanglement. This unified approach bridges nonlinear quantum optics with correlated photonic matter, offering a versatile platform for both theoretical studies and technological applications.

This article is organized as follows. In Sec. II, we introduce the model of excited TLEs coupled to a nonlinear waveguide. We derive an effective non-local interaction Hamiltonian for this system and formalize the concept of the PGA, which captures the underlying multi-point

scattering potential. In Sec. III, we employ scattering theory to analytically obtain the output state when an incident single photon scatters off an excited TLE. We present numerical validation of these predictions and the PGA framework in Sec. III D. In Sec. IV, we demonstrate the formation of spatially separated multi-photon wavepackets resulting from photon-number-dependent group velocities. Using an RGA configuration, we show full-range tunability of the conversion efficiency and uni-directional photon conversion. In Sec. V, we present the cascaded inelastic scattering process, yielding a programmable superposition of spatiotemporally isolated correlated quantum states. We conclude with a summary and an outlook in Sec. VI.

II. MODEL

A. Excited two-level emitters coupled to a nonlinear waveguide

We consider excited TLEs coupled to a nonlinear waveguide, consisting of an array of N coupled nonlinear cavities, as shown in Fig. 1(a). In the frame rotating with the cavity frequency ω_c , the waveguide Hamiltonian is $(\hbar = 1 \text{ throughout this article})$

$$H_w = -\sum_n \left[J(a_n^{\dagger} a_{n+1} + \text{H.c.}) + \frac{U}{2} a_n^{\dagger} a_n^{\dagger} a_n a_n \right], \quad (2)$$

where a_n (a_n^{\dagger}) is the bosonic annihilation (creation) operator for the *n*th cavity, J is the hopping rate between adjacent cavities, and U is the on-site Kerr nonlinear potential, which induces photon-photon interactions within each cavity.

In a linear waveguide (U = 0), photons propagate freely without interaction. In the strong-interaction limit $U/J \rightarrow \infty$, however, photons undergo fermionization and obey an effective exclusion principle [35]. A finite nonlinear potential can lead to the formation of bound states in which multiple photons become localized, forming multi-photon quasiparticles [25, 36], commonly referred to as boson stacks [14], close dimers [26], or photon molecules [37]. For attractive interactions, these quasiparticle states lie below the uncorrelated photon bands, indicating effective binding. As illustrated in Fig. 1(b), the energy spectrum of the nonlinear waveguide reveals a hierarchy of correlated few-photon states: two-photon (doublon) and three-photon (triplon) states emerge progressively below the uncorrelated single-particle band, forming a sequence of bound states caused by the photonphoton interaction [14].

The single-photon states are described by the dispersion relation

$$E_k = -2J\cos(k),\tag{3}$$

with k being the photon momentum. In the relative and center-of-mass coordinates, i.e., $r_c = n_1 - n_2$ and $x_c = n_1 - n_2$

 $(n_1 + n_2)/2$, the dispersion relation of the doublon states is [25, 26]

$$E_K = -\sqrt{U^2 + [4J\cos(K/2)]^2},$$
 (4)

where K denotes the center-of-mass momentum of the photon pair.

For the multi-photon states, the on-site nonlinearity (at $r_c = 0$) acts as an effective impurity, leading to an exponentially localized wave function in the relative coordinate. As a result, the two photons in the doublon state are bunched over a characteristic localization length $L_u(K)$ and propagate as a quasiparticle along the waveguide. The corresponding wave function takes the form

$$\Psi_K(x_c, r_c) = e^{iKx_c} u_K(r_c), \quad u_K(r_c) = u_0 e^{-|r_c|/L_u(K)},$$
(5)

where u_0 is a normalization constant [25, 38, 39]. In the three-photon subspace, a bound quasiparticle state (the triplon) emerges with dispersion relation $E_{\mathcal{K}}$, where \mathcal{K} is the total momentum wave vector [27, 40]. We denote the creation operators for single-photon, doublon, and triplon states as a_k^{\dagger} , D_K^{\dagger} , and T_K^{\dagger} , respectively.

By adding the emitters and their coupling to the waveguide, still in the frame rotating with ω_c , the total system Hamiltonian is

$$H = H_0 + H_{\text{int}},\tag{6}$$

$$H_0 = H_w + \sum_i \frac{\Delta_{ei}}{2} \sigma_i^z, \tag{7}$$

$$H_{\text{int}} = \sum_{i} g_i \sigma_i^- a_{n_i}^{\dagger} + \text{H.c.}, \qquad (8)$$

where σ_i^z and σ_i^{\pm} are the Pauli operators for the *i*th two-level emitter, $\Delta_{ei} = \omega_{ei} - \omega_c$ is the detuning of its transition frequency ω_{ei} from ω_c , n_i denotes its coupling site, and g_i is its coupling strength. The excited and ground states of each emitter are denoted by $|e\rangle$ and $|g\rangle$, respectively.

B. Scope of the study and initial conditions

We consider a scattering scenario, in which an incident single-photon plane wave

$$|\psi\rangle = \exp(ik_0x) \tag{9}$$

propagates from left to right and scatters off a far detuned, initially excited emitter located at n_0 , as shown in Fig. 2(a). In this setup, the nonlinearity of the waveguide enables an inelastic scattering process, in which the incoming single photon is converted into a correlated multiphoton state.

The two-photon state of the considered wQED system

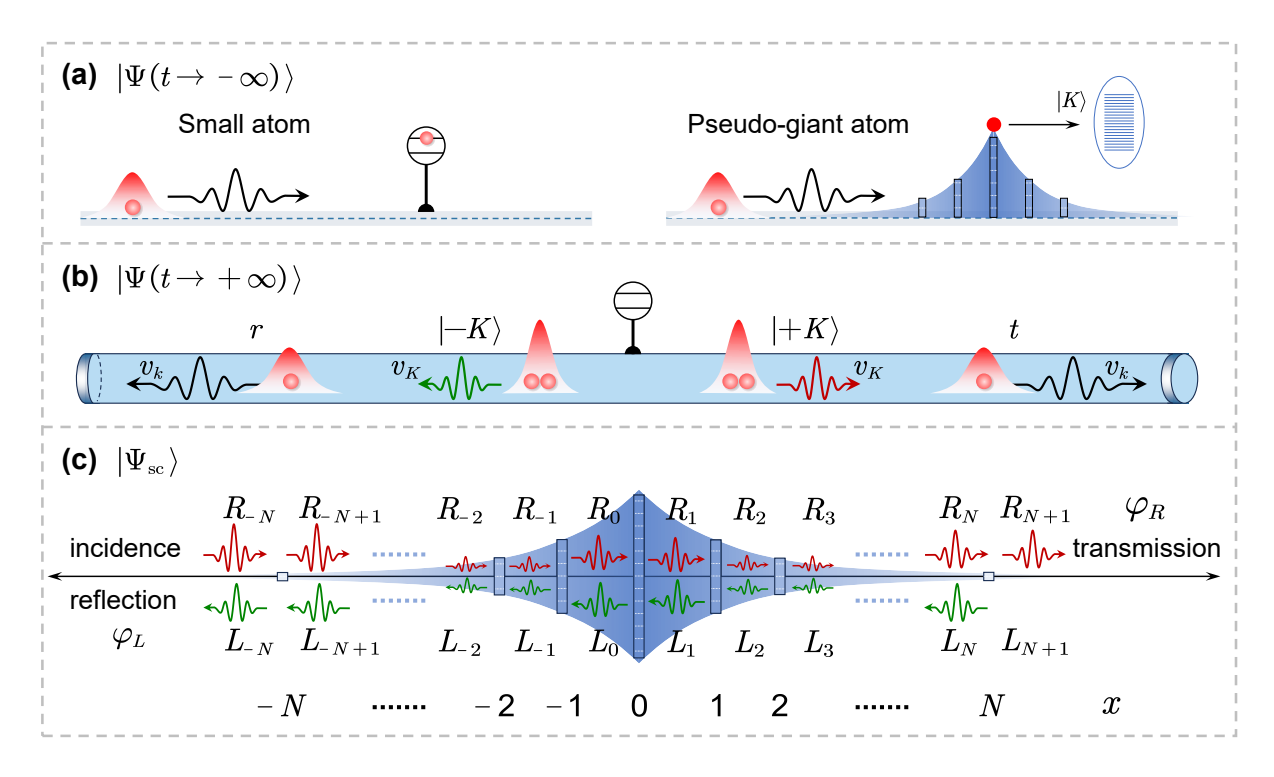


FIG. 2. Schematic illustration of the scattering process at different stages. (a) Initial state at $t \to -\infty$. The left panel shows the physical setup in real space. The right panel depicts the effective "pseudo-giant atom" (PGA) description of the setup. (b) Final state at $t \to +\infty$, featuring the transmitted (t) and reflected (r) single-photon components, as well as right- and left-going doublon wavepackets $|\pm K\rangle$. (c) Scattering eigenstate structure, with right- and left-going single-photon wave functions denoted by $\varphi_{R,L}$. The labeled amplitudes indicate the spatial distribution of waves in different regions.

can be written as

$$|\Psi(t)\rangle = \sum_{n_1, n_2} c_{\text{uc}}(t) |\psi_{\text{uc}}(n_1, n_2)\rangle + \sum_{K} c_K(t) |K\rangle + \sum_{n} c_{e,n}(t) |e, n\rangle,$$
 (10)

where $c_{\rm uc}$ is the probability amplitude for finding two uncorrelated photons at sites n_1 and n_2 , with $|\psi_{\rm uc}(n_1, n_2)\rangle$ the corresponding wave function [26]¹. The amplitude $c_{e,n}$ corresponds to the state with a single photon at site n and the emitter being excited, while $c_K(t)$ represents the amplitude for the doublon mode $|K\rangle$.

In general, when the transition frequency of a TLE lies within the single-photon energy band, the TLE can resonantly exchange photons with the waveguide, enabling emission and absorption. In this regime, the TLE acts as a nonlinear impurity that blocks double occupancy, allowing at most one photon to occupy its site. This effective on-site repulsion gives rise to few-photon bound states. For a detailed discussion of such bosonic impurity models, we refer the interested reader to Ref. [41].

Previous works have harnessed these correlated states to generate nonclassical light, typically by combining multiple emitters [33] or strong coupling schemes [34] to overcome the limited nonlinearity (i.e., shallow optical depth) inherent to a single TLE.

In our proposal, by contrast, the emitter is far detuned from the single-photon band, i.e., $|\Delta_e| \gg 2J$, which strongly suppresses resonant photon exchange. Both spontaneous and stimulated emission are inhibited. The uncorrelated scattering component $c_{\rm uc}$ can be safely adiabatically eliminated, i.e., $c_{\rm uc} \simeq 0$, and the emitter is frozen in its excited state, as shown in Fig. 1(c) at the initial moment. By neglecting the uncorrelated part, the Hilbert space is simplified as

$$|\Psi(t)\rangle \simeq \sum_{K} c_K(t) |K\rangle + \sum_{n} c_{e,n}(t) |e,n\rangle.$$
 (11)

Given $|\Delta_e| \gg 2J + g$, the emitter virtually participates in the formation of a bound state, with negligible population transfer to the ground state [42]. Consequently, the initial state is well approximated by

$$|\Psi(t \to -\infty)\rangle \simeq \sum_{n} e^{ikn} |e, n\rangle.$$
 (12)

Additionally, in the nonlinear bath, the dynamics of the emitter depend not only on the energy structure,

¹ This component is often referred to as the two-photon scattering state in the literature. To avoid confusion with the scattering states involved in the dynamical scattering process discussed later, we refer to it here as the uncorrelated state.

but also on the photon state of the bath, owing to the photon-photon interactions [43, 44]. In contrast to the linear regime, the nonlinear waveguide supports intrinsic multiphoton bound states, providing new channels for light-matter interaction. As shown in Fig. 1(b), we consider a configuration in which the sum of the incident single-photon energy and the far detuned emitter transition frequency lies in the doublon band. Under this energy-matching condition, the incident photon unfreezes the emitter, enabling the joint creation of a two-photon bound state—a doublon.

C. Interaction Hamiltonian: converting single-point interaction into a pseudo-giant atom

We now derive the effective interaction Hamiltonian between the $|e,n\rangle$ and $|K\rangle$ states. Starting from the general case, under the dipole approximation [45], the emitter couples to the waveguide at a single site n_0 , behaving as a point-like impurity [see the left panel of Fig. 2(a)]. The interaction Hamiltonian is then

$$H_{\rm int} = g\sigma^- a_{n_0}^\dagger + g\sigma^+ a_{n_0}, \tag{13}$$

which describes the emission or absorption of a photon at n_0 via transitions between the emitter's excited $|e\rangle$ and ground $|g\rangle$ states [45].

When the total energy of the photon and the emitter lies within the doublon band, a resonant process occurs: the simultaneous annihilation of the incident photon and decay of the emitter jointly excite a doublon mode $|K\rangle$. To describe this process, we project the interaction Hamiltonian in Eq. (13) onto the reduced Hilbert space in Eq. (11). The matrix element for the transition $|e, n\rangle \rightarrow |K\rangle$ is [38, 39, 44]

$$\langle K|\sigma^{-}a_{n_0}^{\dagger}|e,n\rangle = \langle \operatorname{vac}|D_K a_n^{\dagger} a_{n_0}^{\dagger}|\operatorname{vac}\rangle = M^*(K,n,n_0).$$
(14)

Here, $M(K, n, n_0) = \langle \text{vac} | a_n a_{n_0} D_K^{\dagger} | \text{vac} \rangle$ denotes the overlap between the doublon state and the two-photon state $|n, n_0\rangle$, given by [using Eq. (5)]

$$M(K, n, n_0) = \frac{\sqrt{2}}{\sqrt{N}} u_0 e^{iK(n+n_0)/2} e^{-\frac{|n-n_0|}{L_u(K)}}.$$
 (15)

Recall that $L_u(K)$ is the correlated length of the doublon wave function in the relative coordinate $r_c = n - n_0$, characterizing the spatial extent over which the two photons are bound. The transition amplitude is significant only when the separation between the mobile photon (at n) and the emitter site (n_0) is smaller than $L_u(K)$, i.e., $|r_c| = |n - n_0| < L_u(K)$, ensuring sufficient wave function overlap. For simplicity and without loss of generality, we set $n_0 = 0$. The effective interaction Hamiltonian then

becomes

$$H_{\text{int}} = \sum_{K,n} g M^*(K, n, 0) |K\rangle \langle e, n| + \text{H.c.}$$

$$= \sum_{K,n} \frac{g_n}{\sqrt{N}} e^{-iKn/2} D_K^{\dagger} \sigma_- a_n + \text{H.c.}$$
(16)

where $g_n = \sqrt{2}gu_0 \exp\left[-|n|/L_u(K)\right]$.

In contrast to the scattering process for a point-like emitter in linear waveguides [46–49], this effective interaction Hamiltonian captures two distinct physical aspects, corresponding to the summations over the doublon momentum K and the photon position n:

- 1. The emitter mediates a nonlinear scattering process that converts an incident single photon with wave vector k into a propagating two-photon bound state $|K\rangle$. Unlike conventional scattering, the incident photon does not scatter off a single mode $(|e\rangle$ or $|g\rangle$), but off the entire available spectrum of correlated two-photon states.
- 2. Owing to the exponential localization of the doublon wave function, the transition amplitude is significant only when the incident photon is within a distance of the emitter $|n n_0| < L_u(K)$. Thus, $L_u(K)$ sets the effective interaction range, defining the spatial scale over which the scattering process becomes appreciable. Consequently, the photon does not scatter off a point-like emitter, but off an extended, nonlocal scattering potential.

In Eq. (13), the emitter is modeled under the dipole approximation as having a point-like coupling to the waveguide, characterized by a local interaction strength g. However, in the effective Hamiltonian in Eq. (16), the scattering process is inherently nonlocal, involving contributions from multiple sites. The coupling strength at each site n is weighted by the spatial profile of the doublon wave function, yielding an effective site-dependent amplitude g_n . This multi-point coupling structure resembles that of a *giant atom*, which couples to the waveguide at multiple points [28–32, 50]. Therefore, within the nonlinear scattering framework, the originally pointcoupled TLE can be reinterpreted as a "pseudo-giant atom" (PGA) with a spatially distributed coupling profile and a continuum of internal modes, as shown in the right panel of Fig. 2(a).

III. NONLINEAR SCATTERING THEORY WITH PSEUDO-GIANT ATOM FORMULA

A. Introduction to the scattering process: general overview and theoretical framework

To solve the scattering problem of a propagating single photon interacting with a TLE, we employ standard scattering theory based on the Lippmann–Schwinger formalism [46, 51]. Here, we provide a brief overview of the scattering process, as shown in Fig. 1(c). As $t \to -\infty$, the incoming state $|i\rangle$ is a free state far from the interaction region and governed by H_0 [see Eq. (7)]. Simultaneously, the emitter is highly detuned from the single-photon modes, suppressing spontaneous emission.

Due to the nonlocal scattering potential, the scattering initiates at the outer edges of the PGA, where the interaction is weak but finite. As the incident photon propagates toward the center of the coupling region, the effective interaction strength increases gradually. The interaction then decreases symmetrically as the photon exits through the opposite edge of the PGA. In Fig. 1(c), the shaded blue region depicts the non-local scattering potential, as governed by the interaction Hamiltonian in Eq. (16). During this process, part of the incident single photon hybridizes with the emitter to form a propagating doublon state, while the remainder is either transmitted or reflected.

Consequently, at $t \to +\infty$, the final state $|f_i\rangle$ is a free state governed by H_0 , far away from the interaction regime. Note that the final state contains not only single-photon, but also doublon components, as shown in Fig. 2(b). The subscript i indicates that the final state depends on the incoming state.

The interaction Hamiltonian is non-local, yet its range is confined within the correlation length of the doublon wave function. Thus, the incoming photon interacts with the emitter only during a short time interval before propagating away. Scattering theory remains applicable: the interaction can be treated as being adiabatically "switched on" as $t \to 0$, reaching its peak strength at t = 0, and then being adiabatically "switched off" as $t \to +\infty$ [46, 51].

We denote the interacting scattering state at t=0 by $|\Psi_{\rm sc}\rangle$. The three relevant states satisfy the Lippmann–Schwinger equations

$$|\Psi_{\rm sc}\rangle = |i\rangle + \frac{1}{E - H_0 + i0^+} H_{\rm int} |\Psi_{\rm sc}\rangle,$$
 (17)

$$|\Psi_{\rm sc}\rangle = |f_i\rangle + \frac{1}{E - H_0 - i0^+} H_{\rm int} |\Psi_{\rm sc}\rangle, \qquad (18)$$

where $(E-H_0\pm i0^+)^{-1}\equiv G_0^{R/A}$ are the free retarded and advanced Green's functions, respectively. These equations describe the time evolution of the system in complementary directions: Eq. (17) corresponds to forward evolution from the initial state $|i\rangle$ to the scattering state $|\Psi_{\rm sc}\rangle$, mediated by G_0^R under the adiabatic turn-on of the interaction; Eq. (18) describes the backward evolution from the final state $|f_i\rangle$ to $|\Psi_{\rm sc}\rangle$, governed by G_0^A during the adiabatic turn-off. Together, Eqs. (17) and (18) imply the eigenvalue relations $H_0|i\rangle=E|i\rangle$, $H|\Psi_{\rm sc}\rangle=E|\Psi_{\rm sc}\rangle$, and $H_0|f_i\rangle=E|f_i\rangle$, where E is the

total energy of the system.

Note that the scattering state connects the incoming state to the final state, mediated by $G_0^{R/A}$. Given a specific incoming state, the energy is fixed by $H_0 |i\rangle = E |i\rangle$. The scattering state is then obtained via solving the secular equation $H |\Psi_{\rm sc}\rangle = E |\Psi_{\rm sc}\rangle$. The corresponding final state $|f_i\rangle$ follows directly from the Lippmann–Schwinger equation in Eq. (18).

B. Scattering eigenstates

To proceed, we determine the scattering state $|\Psi_{\rm sc}\rangle$ by solving the secular equation in real space. An equivalent formulation in momentum space, which yields identical results, is presented in the Appendix A. To characterize the propagation dynamics of single photons, we project the Hamiltonian onto the basis in Eq. (11) and express it in continuous form via linearization around k [46, 52, 53]:

$$H_0 \simeq \int dx \, iv_k \left[-c_R^{\dagger}(x) \frac{\partial}{\partial x} c_R(x) + c_L^{\dagger}(x) \frac{\partial}{\partial x} c_L(x) \right] + \frac{\Delta_e}{2} \sigma_z + E_K D_K^{\dagger} D_K, \tag{19}$$

and the interaction Hamiltonian is

$$H_{\text{int}} = \int dx \left\{ \sum_{K,n} g M^*(K,n,0) \delta(x,n) \right.$$
$$D_K^{\dagger} \sigma_{-} [c_R(x) + c_L(x)] + \text{H.c.} \right\}. \tag{20}$$

Here, $a_x \simeq c_R(x) + c_L(x)$, where $c_{R/L}$ are bosonic operators which create a right- or left-going photon at position x, and v_k is the group velocity of the single photon. The Hamiltonian in Eq. (19) conserves particle number, and the scattering state takes the form

$$|\Psi_{\rm sc}\rangle = \int dx \Big[\varphi_R(x)c_R^{\dagger}(x) + \varphi_L(x)c_L^{\dagger}(x)\Big]\sigma_+ |0\rangle + \sum_K u_K D_K^{\dagger} |0\rangle, \qquad (21)$$

where $|0\rangle$ is the vacuum state, $\varphi_{R,L}(x)$ is the right-/left-going single-photon wave function, and u_K is the probability amplitude for the doublon state $|K\rangle$ to be excited.

Within the PGA formalism, the interaction Hamiltonian [Eq. (16)] only acts on integer lattice sites. This discrete coupling structure is preserved in Eq. (20), through the delta function $\delta(n,x)$. The summation over n spans the nonlocal scattering region, anchoring the interaction to discrete spatial points. Consequently, the wave function varies only at these points, resulting in piecewise-constant behavior. Specifically, the single-photon wave function remains constant between adjacent lattice sites and changes only at integer positions x = n:

$$\varphi_R(x) = e^{+ikx} \left\{ R_{-N}\Theta[-(x+N)] + \sum_{n=-N+1}^{N} R_n[\Theta(x-n) - \Theta(x-n+1)] + R_{N+1}\Theta(x-N) \right\}, \tag{22}$$

$$\varphi_L(x) = e^{-ikx} \left\{ L_{-N}\Theta[-(x+N)] + \sum_{n=-N+1}^{N} L_n[\Theta(x-n) - \Theta(x-n+1)] + L_{N+1}\Theta(x-N) \right\},$$
(23)

where $\Theta(x)$ is the Heaviside step function. This ansatz is analogous to a scattering process in which a single photon scatters off a *real giant atom* with multiple coupling points [54–56]. The coefficients R_n and L_n denote the probability amplitudes of the wave function in the respective regions, as shown in Fig. 2(c).

Returning to Eq. (17), under the assumption of an initial plane wave, the fore and aft of the wave function are given by

$$R_{-N} = 1$$
, $R_{N+1} = t$ $L_{-N} = r$, $L_{N+1} = 0$, (24)

where the right-going wave function is assumed to be 1 at the position x < N, and t and r are the transmission and reflection amplitudes, respectively. The initial state gives the total energy of the system: $E = \Delta_e + \omega_{k_0} \simeq \Delta_e + v_{k_0} k_0$. Substituting the Hamiltonian in Eq. (19) and the scattering-state ansatz in Eq. (21) into the secular equation $H |\psi\rangle = E |\psi\rangle$, we derive the equations

$$(E_{K_r} - E_K)u_K = \frac{1}{\sqrt{N}} \sum_n g_n e^{-iKn/2} \left[\mathcal{P}_R^+(n) + \mathcal{P}_L^+(n) \right] / 2, \tag{25}$$

$$iv_k \mathcal{P}_R^-(n) = iv_k \mathcal{P}_L^-(n) = \frac{1}{\sqrt{N}} \sum_K g_n e^{iKn/2} u_K,$$
 (26)

where $E_{K_r} = (\Delta_e + \omega_{k_0})$. Here, K_r denotes the resonant doublon mode, and

$$\mathcal{P}_{R}^{\pm}(n) = (R_{n+1} \pm R_n)e^{+ikn},$$
 (27)

$$\mathcal{P}_L^{\pm}(n) = (L_n \pm L_{n+1})e^{-ikn}.$$
 (28)

Equations (25) and (26) reveal that the single-photon mode and the doublon mode are coupled, via the far detuned emitter. First, Eq. (25) describes the conversion of a single photon into a doublon through the pseudocoupling points at integer lattice sites. The effective coupling strength is proportional to $g_n \exp(-iKn/2)$ and depends on the single-photon probability amplitude at these discontinuities. In contrast, Eq. (26) governs the reverse process—the decay of a doublon back into a single photon via the same pseudo-coupling structure.

Under the initial condition, Eq. (25) is transformed into

$$u_K = \frac{1}{\sqrt{N}} \sum_n \frac{g_n e^{-iKn/2}}{E_{K_r} - E_K + i0^+} \frac{\mathcal{P}_R^+(n) + \mathcal{P}_L^+(n)}{2}. \quad (29)$$

The primary task is now to determine the functional forms of $\mathcal{P}_{R/L}^{\pm}(x)$. Substituting Eq. (29) into Eq. (26) eliminates u_K and yields a closed equation for the single-photon wave function:

$$\mathcal{P}_{R/L}^{-}(n) = -\frac{1}{v_k v_{K_r}} \sum_{n'} g_n g_{n'} e^{iK_r |n-n'|/2} \left[\mathcal{P}_R^{+}(n') + \mathcal{P}_L^{+}(n') \right] / 2.$$
(30)

These equations (for arbitrary n) exhibit a convolution structure, arising from the multipoint coupling of the PGA, which acts as an effective nonlocal scattering potential. The scattering response at any given point depends on the cumulative effect across the entire PGA region, rather than on local properties alone. Crucially, this spatially distributed pseudo-coupling gives rise to complex interference effects, discussed in the following section.

In a conventional system with light–matter interaction, an emitter with discrete energy levels couples to a bath with continuous modes, and the dynamics are governed primarily by the bath's density of states, as described by Fermi's golden rule [45]. In contrast, in the present system, the emitter mediates the transition between two quantum fields, the single-photon and the doublon modes. Consequently, the coefficients in Eq. (30) depend on the densities of both continua, $\rho_k = 1/v_{K_r}$.

Note that in Eq. (30), the number of equations matches the number of unknown variables. By solving for $\mathcal{P}_{R/L}^{\pm}(n)$ at $k=k_0$, we determine their values and subsequently obtain the amplitudes of the single-photon wave function (R_n, t, L_n, r) via Eqs. (27) and (28). Substituting $\mathcal{P}_{R/L}^{\pm}(n)$ back into Eq. (25), the doublon amplitude u_k can also be obtained. The solution framework, including the wave-function ansatz [Eqs. (22) and (23)] and the auxiliary variables $\mathcal{P}_{R/L}^{\pm}(n)$ [Eqs. (27) and (28)] can also be applied to the case of a real giant atom (RGA). The key distinction lies in the nature of the scattering potential: in the RGA, it arises from discrete, localized energy levels, whereas in PGA, it stems from continuous, propagating doublon modes.

The overall summation structure reflects the occurrence of multiple scattering events and the interference between distinct scattering pathways. At its core, this equation describes the propagation and interference of

quantum waves in the presence of a nonlocal potential. It further reveals a fundamental connection between scattering theory and the convolution structure. This nonlocal scattering potential is central to the nonlinear scattering behavior observed in this system.

C. The output field for the single-photon plane-wave input

The final state takes the form

$$|f_i\rangle \simeq \int dx [f_R(x)|e, x_R\rangle + f_L(x)|e, x_L\rangle]$$

 $+ \sum_{\pm K} f_{\pm K} |\pm K\rangle,$ (31)

where the doublon mode is separated into positive and negative components to distinguish right- and left-going waves. We have so far obtained the scattering state for a single-photon plane-wave input. To obtain the output state, we return to Eq. (18) and project the final state onto $|e,x_{R/L}\rangle$ and $|K\rangle$, respectively. Here, $f_{R,L,\pm K}$ denote the probability amplitudes of right-/left-going single-photon and doublon modes in the final state, as shown in Fig. 2(b).

1. Doublon component

Substituting the interaction Hamiltonian in Eq. (20) and the scattering state in Eq. (21) into Eq. (18), and projecting onto the $|+K\rangle$ state, we obtain

$$\langle +K|f\rangle = \langle +K|\Psi_{\rm sc}\rangle - \langle +K|\frac{1}{E_{K_r} - H_0 - i0^+} H_{\rm int} |\Psi_{\rm sc}\rangle \quad (32)$$

$$= \frac{1}{\sqrt{N}} \sum_{x} \sum_{K'} g_n \mathcal{P}_{R+L}^+(n)$$

$$\langle +K|\frac{e^{-iK'n/2}}{E_{K_r} - E_{K'} + i0^+} - \frac{e^{-iK'n/2}}{E_{K_r} - E_{K'} - i0^+} |K'\rangle . \quad (33)$$

The two Green's function integrals are [51]

$$\begin{split} &\frac{1}{N}\sum_{K}\frac{e^{-iKn/2}}{E_{K_r}-E_K+i0^+}\left|K\right\rangle = -\frac{i}{v_{K_r}}\times\\ &\left[e^{-iK_rn/2}\Theta(-n)\left|+K_r\right\rangle + e^{+iK_rn/2}\Theta(+n)\left|-K_r\right\rangle\right],\ (34)\\ &\frac{1}{N}\sum_{K}\frac{e^{-iKn/2}}{E_{K_r}-E_K-i0^+}\left|K\right\rangle = +\frac{i}{v_{K_r}}\times\\ &\left[e^{-iK_rn/2}\Theta(+n)\left|+K_r\right\rangle + e^{+iK_rn/2}\Theta(-n)\left|-K_r\right\rangle\right].\ (35) \end{split}$$

In the integrals, we apply the Wigner–Weisskopf approximation, in which E_K is linearized around $K = K_r$ [45].

The resulting equations provide an intuitive physical picture. The first term in Eq. (32) describes the evolution of the incident single photon from $t=-\infty$ to t=0, governed by the retarded Green's function. The propagator G_0^R yields a contribution from the nonlocal scattering potential in the region x<0, represented by $\Theta(-x)$ in Eq. (34), as the wave propagates forward in time from $x=-\infty$ to x=0. The second term describes evolution from $t=\infty$ to t=0, governed by the advanced Green's function G_0^A . In this case, G_0^A accounts for the influence of the scattering potential in the region x>0, captured by $\Theta(+x)$ in Eq. (35), as the wave evolves backward in time from $x=+\infty$ to x=0. Combining both spatial directions, the initial state evolves under the complete nonlocal potential.

The final state is then given by

$$f_{+K_r} = \langle +K_r | f \rangle$$

$$= -\frac{i}{v_{K_r}} \sum_{n} g_n \mathcal{P}_{R+L}^+(n) [\Theta(-n) + \Theta(+n)] e^{-iK_r x/2}$$

$$= -\frac{i}{v_{K_r}} \sum_{n} g_n \mathcal{P}_{R+L}^+(n) e^{-iK_r n/2}.$$
(36)

To make the expression more concise, we here defined

$$\mathcal{P}_{R+L}^{+}(n) = \frac{\mathcal{P}_{R}^{+}(n) + \mathcal{P}_{L}^{+}(n)}{2}.$$
 (37)

For the left-going doublon mode -K, the first (second) term yields $\Theta(+n)$ $[\Theta(-n)]$:

$$f_{-K_r} = \langle -K_r | f \rangle = -\frac{i}{v_{K_r}} \sum_n g_n \mathcal{P}_{R+L}^+(n) e^{+iK_r n/2}.$$
 (38)

Up to now, we obtained the probability amplitudes for the $\pm K_r$ doublon modes. Note that, for the input singlephoton state $|i\rangle$, it is straightforward to show that

$$\langle \pm K | i \rangle = \langle \pm K | \Psi_{\rm sc} \rangle - \langle \pm K | \frac{1}{E_{K_r} - H_0 + i0^+} H_{\rm int} | \Psi_{\rm sc} \rangle.$$
(39)

The first term is identical to the $|f_i\rangle$ state, while the second term takes the retarded form $1/(E_{K_r}-E_K+i0^+)$, which coincides with the first, i.e.,

$$\langle \pm K | i \rangle = 0. \tag{40}$$

The process can be seen as the evolution from $t = -\infty$ to t = 0, followed by a return to $t = -\infty$, effectively reconstructing the initial state.

2. Single-photon component

Next, we derive the single-photon transmission and reflection amplitudes by projecting onto $|e, x_{R/L}\rangle$:

$$f_{R} = \langle e, x_{R} | f \rangle$$

$$= \langle e, x_{R} | \Psi_{sc} \rangle - \langle e, x_{R} | \frac{1}{E_{K_{r}} - H_{0} - i0^{+}} H_{int} | \Psi_{sc} \rangle$$

$$= \varphi_{R}(x) - \int dx' \sum_{n} i v_{k} \mathcal{P}_{R}^{-}(n) \delta(x' - n) \langle x_{R} | \frac{1}{E_{K_{r}} - H_{0} - i0^{+}} | x_{R}' \rangle$$

$$= \varphi_{R}(x) - \frac{1}{v_{k_{0}}} \sum_{n} \mathcal{P}_{R}^{-}(n) e^{+ik_{0}(x-n)} \Theta(n-x), \qquad (41)$$

and f_L can be similarly obtained as

$$f_L = \varphi_L(x) - \frac{1}{v_{k_0}} \sum_n \mathcal{P}_L^-(n) e^{-ik_0(x-n)} \Theta(x-n).$$
 (42)

During the derivation, we employ the Fourier transform to obtain the Green's function integral

$$\langle x | \frac{1}{E_{K_r} - H_0 - i0^+} | x' \rangle = \frac{1}{2\pi} \int dk \frac{e^{ik(x-x')}}{\omega_{k_0} - \omega_k - i0^+}$$

$$= \begin{cases} (i/v_{k_0})e^{+ik_0(x-x')}\Theta(x'-x)|_{+k_0} \\ (i/v_{k_0})e^{-ik_0(x-x')}\Theta(x-x')|_{-k_0} \end{cases} . \tag{43}$$

Note that this is the advanced Green's function, describing evolution from $t=+\infty$ to t=0. Consequently, the response at position x due to the excitation at x' is mediated by the right-going mode +k when x'>x, and by the left-going mode -k when x'< x. By substituting the wave-function ansatz [Eqs. (22) and (23)] into the expressions for the final state [Eqs. (41) and (42)], and carefully analyzing the solution in each piecewise region, we obtain the single-photon components of the initial and final states:

$$\langle e, x | i \rangle = e^{ik_0 x},\tag{44}$$

$$\langle e, x | f_i \rangle = t e^{ik_0 x} + r e^{-ik_0 x}, \tag{45}$$

where $t = f_R$ and $r = f_L$ denote the transition and reflection amplitudes, respectively, of the single photon.

Equations (40) and (44) confirm that the ansatz [Eq. (21)] is a scattering eigenstate under the given initial condition. Ultimately, we obtain the final state, described by Eqs. (36), (38), and (45), for an incident single-photon plane wave $\exp(ik_0x)$.

3. Flux conservation

In the waveguide, the energy carried by a wave packet propagates at the group velocity [57, 58]. The energy flux j can be approximated as the product of the amplitude of the wave packet and its group velocity, i.e., $j = Pv_q$. In

conventional wQED, most studies focus on single-photon scattering, where both the incident and final states contain only single-photon components. This leads to the familiar flux-conservation relation $t^2+r^2=1$ [46, 48]. However, in our proposal, the single photon can be inelastically scattered into a doublon mode, with a different group velocity, i.e., $v_k \neq v_K$. As a result, flux conservation must account for contributions from both single-photon and doublon excitations. Now, the conservation law takes the form

$$v_k P_S^i + v_K P_D^i = v_k P_S^f + v_K P_D^f, (46)$$

$$v_k = v_k (t^2 + r^2) + v_K \sum_{\pm} |u_{\pm K_r}|^2,$$
 (47)

where $P_{S/D}^{i/f}$ denote the single-photon and doublon population in the initial and final state, respectively. We refer interested readers to Ref. [59] for a more detailed discussion of probability currents in systems with position-dependent velocity.

The incident wave packet is assumed to be a single photon with unit population in our numerical simulations. Consequently, in order to satisfy flux conservation, the final state is written as [35, 59]

$$|f_{i}\rangle = \sum_{x} \left(te^{+ik_{0}x} + re^{-ik_{0}x}\right)|e, x\rangle + \sqrt{\frac{v_{K_{r}}}{v_{k_{0}}}} u_{\pm K_{r}}|\pm K_{r}\rangle.$$

$$(48)$$

The group-velocity factor arises from the distinct dispersion relations (E_k, E_K) , and serves as a critical precursor to spatiotemporal photon-number-dependent sorting.

D. Multi-point scattering and interference within the PGA framework

We consider an incident wave packet centered at momentum k_0 with a spectral width L_G . Analogous to spontaneous emission and under the Wigner-Weisskopf approximation, i.e., $L_G \ll 4J$, the final state is dominated by spectral components near k_0 , and remains insensitive to the temporal envelope of the input, as further discussed in Appendix B. This behavior contrasts fundamentally with stimulated emission from an initially excited TLE, where the output field depends on the spectral and temporal profile of the input due to the finite emission linewidth Γ [47].

To validate the PGA formula, we numerically simulate the evolution of a Gaussian wave packet governed by the full Hamiltonian [Eq. (6)]. The incident wave packet is given by

$$\psi_G(k) = \left(\frac{1}{2\pi L_G^2}\right)^{\frac{1}{4}} \exp\left[-\frac{(k-k_0)^2}{4L_G^2}\right]. \tag{49}$$

Its Fourier transform yields a spatially localized single-photon state centered at x_0 . In the limit $L_G \to 0$ (narrow momentum spread), it approximates a plane wave.

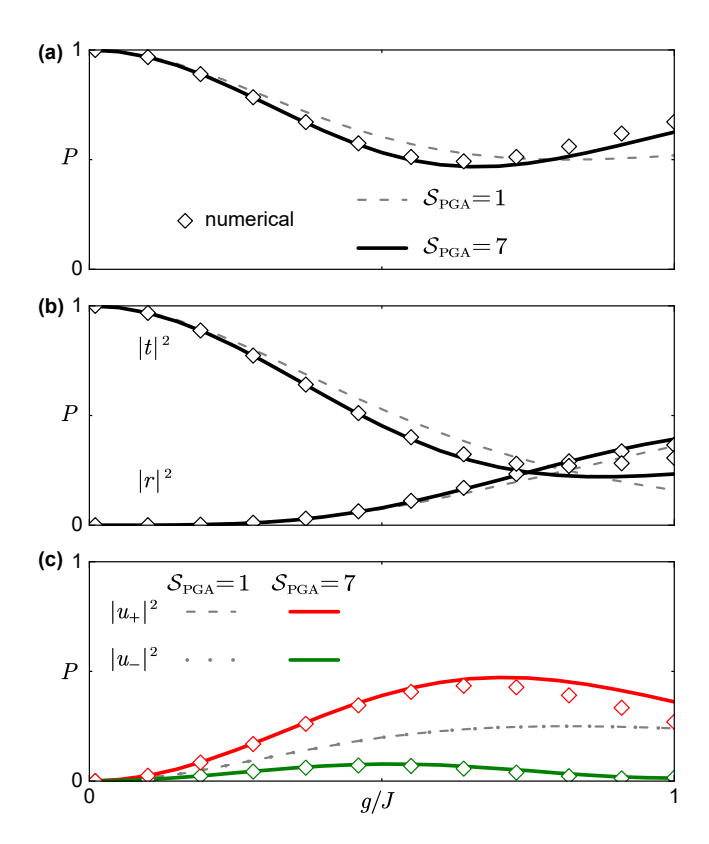


FIG. 3. Populations of (a) the emitter excitation, (b) single-photon transmission $|t|^2$ and reflection $|r|^2$, and (c) right-and left-going doublons $|u_{\pm}|^2$, as functions of the coupling strength g. Numerical results are indicated by diamond markers. Solid colored curves are obtained by solving Eq. (48) with the size of the PGA $S_{\rm PGA}=7$, while thin gray dashed curves represent the pointlike scenario $S_{\rm PGA}=1$. Parameters are $L_G=0.002$, U=6J, $\Delta_e=-6.633J$, and $k_0=\pi/2$.

We set the waveguide length to N=2000, resulting in a Hilbert-space dimension of $N_H \simeq N^2/2 = 2 \times 10^6$. Figure 3 displays the populations of key physical quantities as functions of g. These quantities include the emitter excitation, single-photon transmission $|t|^2$ and reflection $|r|^2$, and right- and left-going doublon populations $|u_{\pm}|^2$. Owing to the strong binding of the doublon, the numerical simulation results are defined as

$$|t|^2/|r|^2 = \sum_{n\neq 0} |c_{e,n}|^2, \quad |u_{\pm}|^2 = \sum_{x_c\neq 0, r=0, 1, 2} |c_{x_c, r}|^2.$$
 (50)

The two-photon state is dominated by the doublon component, with negligible contributions from uncorrelated photon pairs, thereby justifying the approximation $c_{\rm uc} \simeq 0$.

The analytical results are given by Eq. (48). We first consider the "pointlike" scenario, in which only the local term $\delta(n, n_0)M(K, n, n_0)$ is retained [the size of the PGA $\mathcal{S}_{PGA} = 1$; see Fig. 4(a)], corresponding to the gray dashed curves in Fig. 3. Within this approximation, the doublon distribution is symmetric, with all doublons formed at $r_c = 0$ [48]. However, as shown in Fig. 3(c), the

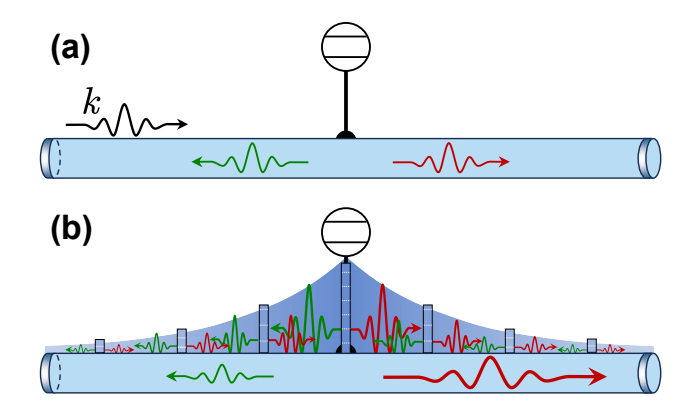


FIG. 4. Schematic illustration of interference in doublon generation. (a) The pointlike scenario with equal distribution doublons in the right- and left-going modes. (b) PGA scenario: interference among seven pseudo-coupling points leads to an asymmetric doublon distribution.

numerical results exhibit a distinctly asymmetric doublon distribution. This clear discrepancy demonstrates that the pointlike approximation fails to capture the essential physics of this process.

Therefore, to obtain an accurate analytical description of this nonlinear scattering process, it is essential to incorporate the effective pseudo-multiple coupling points of the PGA. Due to the exponential spatial decay $\exp[-|r_c|/L_u(K)]$, the transition amplitude $M(K_r, n, n_0)$ becomes negligible for $r_c = |n - n_0| > L_u(K)$. Specifically, we truncate the range of PGA at $r_c = 3$, retaining seven pseudo-coupling points at $n=0,\pm 1,\pm 2,\pm 3$ [i.e., $S_{PGA} = 7$; see Fig. 4(b)]. By solving the coupled system of equations in Eq. (30) and following the analytical derivation, we obtain the final state given by Eq. (48). Figure 3 shows the agreement between the analytical results (solid colored curves) and full dynamical simulations (diamonds), which validates the PGA framework. Crucially, at each pseudo-coupling point, the doublon is generated symmetrically in both directions with amplitudes and phases; see Fig. 4(b). Analogous to the multipoint interference in real giant atoms [50], the doublons generated at different spatial positions interfere coherently, which results in an asymmetric doublon distribution between the left- and right-going directions, i.e., $|u_{+K_r}|^2 \neq |u_{-K_r}|^2$.

In this physically local single-point coupling scenario, the nonlocal doublon wave function underpins effective multipoint scattering dynamics within the PGA framework, enabling coherent interference and leading to directional asymmetry. Although multiple interference pathways coexist, the effective coupling strength at each pseudo-site scales linearly with the physical coupling $g_n \propto g$, thereby limiting the degree of tunability. As a result, scattering is dominated by the central channel at n=0, since $g_{n=0}\gg g_{n\neq 0}$. As shown in Fig. 3, the conversion efficiency reaches a maximum, yet a finite dou-

blon population persists in the incident direction. Thus, achieving flexible modulation of doublon generation and realizing optimal unidirectional cascaded scattering remain challenges.

IV. SPATIALLY SEPARATED PHOTONIC WAVE PACKETS SORTED BY PHOTON NUMBER

To further investigate the scattering dynamics, we show in Fig. 5(a) the time evolution of key state populations for U=0J and 6J, including: the single-photon probability $P_{\rm I}=\sum_n|c_{e,n}|^2$; the doublon population $P_D=\sum_{x_c,r_c=0,1,2}|c_{x_c,r}|^2$ (restricted to tightly bound states with $r_c\leq 2$); and the total two-photon population $P_{\rm II}=\sum_{n_1,n_2}|c_{n_1,n_2}|^2$, which encompasses both doublon and uncorrelated components. For U=0, the incident single photon passes freely by the emitter without interaction and no doublon states are formed, leaving $P_{\rm I}\simeq 1$ and $P_{\rm II}=|c_{\rm uc}|^2\simeq 0$ throughout the evolution. In contrast, for U=6J, the single photon cooperates with the emitter to jointly form a doublon state. Importantly, comparison between the U=0 and U=6J cases reveals that over the entire process, the excitation into uncorrelated states is negligible, and the two-photon component is dominated by the doublon, with $P_{\rm II}\simeq P_D$.

A. Spatial separation of scattered wavepackets

To characterize the photon field, Fig. 5(b) shows the expectation value of the photon number as a function of position n and time t, defined by

$$\langle \mathcal{N} \rangle = \langle \Psi(t) | a_n^{\dagger} a_n | \Psi(t) \rangle, \qquad (51)$$

where $|\Psi(t)\rangle$ is the total two-photon state given by Eq. (10). As the incident single-photon packet scatters off the emitter, the outgoing photonic field splits into four distinct components: the transmitted t and reflected r single-photon components, and the right- and left-going doublon components $|u_{\pm K_r}|^2$, corresponding to the final state in Eq. (48). Figure 5(b) illustrates the natural spatial separation between single-photon and doublon wave packets within the same waveguide. This separation arises because the doublons, as bound two-photon states, propagate at a slower group velocity compared to the free single photons. The disparity in group velocity directly leads to their spatial divergence.

In Ref. [33], the authors achieve spatial separation of multiphoton states through a photon-number-dependent Wigner delay, arising from resonant photon exchange of a TLE. However, owing to the limited optical depth of a single TLE, the induced time delay is small and scales as $\tau_n = 4/(n^2\Gamma)$ for an *n*-photon state traversing the TLE. Consequently, significant temporal delays require either multiple emitters arranged in an ordered array or operation in the strong coupling regime, both of which increase

experimental complexity. By contrast, in our proposal, the nonlinearity is intrinsic to the waveguide bath via the interaction strength U, making the multi-photon bound states inherent to the bath. A single far detuned emitter couples to the nonlinear waveguide and mediates the scattering of an incident single photon into a two-photon bound state, with possible extension to higher-order correlated photon states (see Sec. V). Owing to the distinct group velocities of the scattered single-photon and bound-state components, these quantum excitations naturally separate in space after the interaction, without the need for engineered emitter arrays or strong coupling.

Moreover, the distinct group velocities shape the spatial profiles of the output states. The single-photon profile remains unchanged, while the doublon width is given by $W_D = v_K t_{\rm int} = W_S v_K / v_k$, where $W_S = v_k t_{\rm int}$ is the single-photon width and $t_{\rm int}$ is the interaction duration [see the inset of Fig. 5(b)]. Figure 6 displays the photonic field at Jt = 600, showing a clear spatial separation between the single-photon and two-photon components. The two-photon field exhibits strong spatial correlations, featuring a sharp peak at r = 0 and rapid decay [36, 38, 39]. After the scattering, the single-photon and doublon output states inherit the spatial profile of the incident wave packet, centered at $x = v_{k_0/K_r}t$ with amplitudes given by $|t|^2$, $|r|^2$, and $|u_{\pm}|^2 u_{K_r}(r)$, respectively.

B. Modulating the scattering process with a real giant emitter

Real giant atoms, which couple to the waveguide at multiple points [28–32], possibly with engineered local phases [55, 60], provide enhanced control over light—matter interactions through interference among the coupling points. Leveraging this tunability, we propose an RGA configuration to achieve higher conversion efficiency into doublons and optimal unidirectional distribution. For simplicity and without loss of generality, we consider a giant emitter that couples to the waveguide at two points, n_l and n_r , with local phases ϕ_l and ϕ_r , as shown in Fig. 7(a). The distance between the two coupling points is $d = |n_l - n_r|$. The initial interaction Hamiltonian is then expressed as

$$H_{\rm int} = g\sigma_{-} \left(e^{i\phi_l} a_{n_l}^{\dagger} + e^{i\phi_r} a_{n_r}^{\dagger} \right) + \text{H.c.}$$
 (52)

Following the derivation in Sec. II C, the effective interaction Hamiltonian becomes

$$H_{\text{int}} = \sum_{K,n} \sum_{\tau=l,r} g e^{i\phi_{\tau}} M(K,n,n_{\tau}) D_{K}^{\dagger} \sigma_{-} a_{n} + \text{H.c.}$$

$$= \sum_{K,n} \sum_{\tau=l,r} \frac{g_{|n-n_{\tau}|}}{\sqrt{N}} e^{-iK(n+n_{\tau})/2} e^{i\phi_{\tau}} D_{K}^{\dagger} \sigma_{-} a_{n} + \text{H.c.},$$
(53)

where $g_{|n-n_{\tau}|} = \sqrt{2}u_0ge^{-|n-n_{\tau}|/L_u(K)}$. The physical process can be interpreted as follows: an incident photon

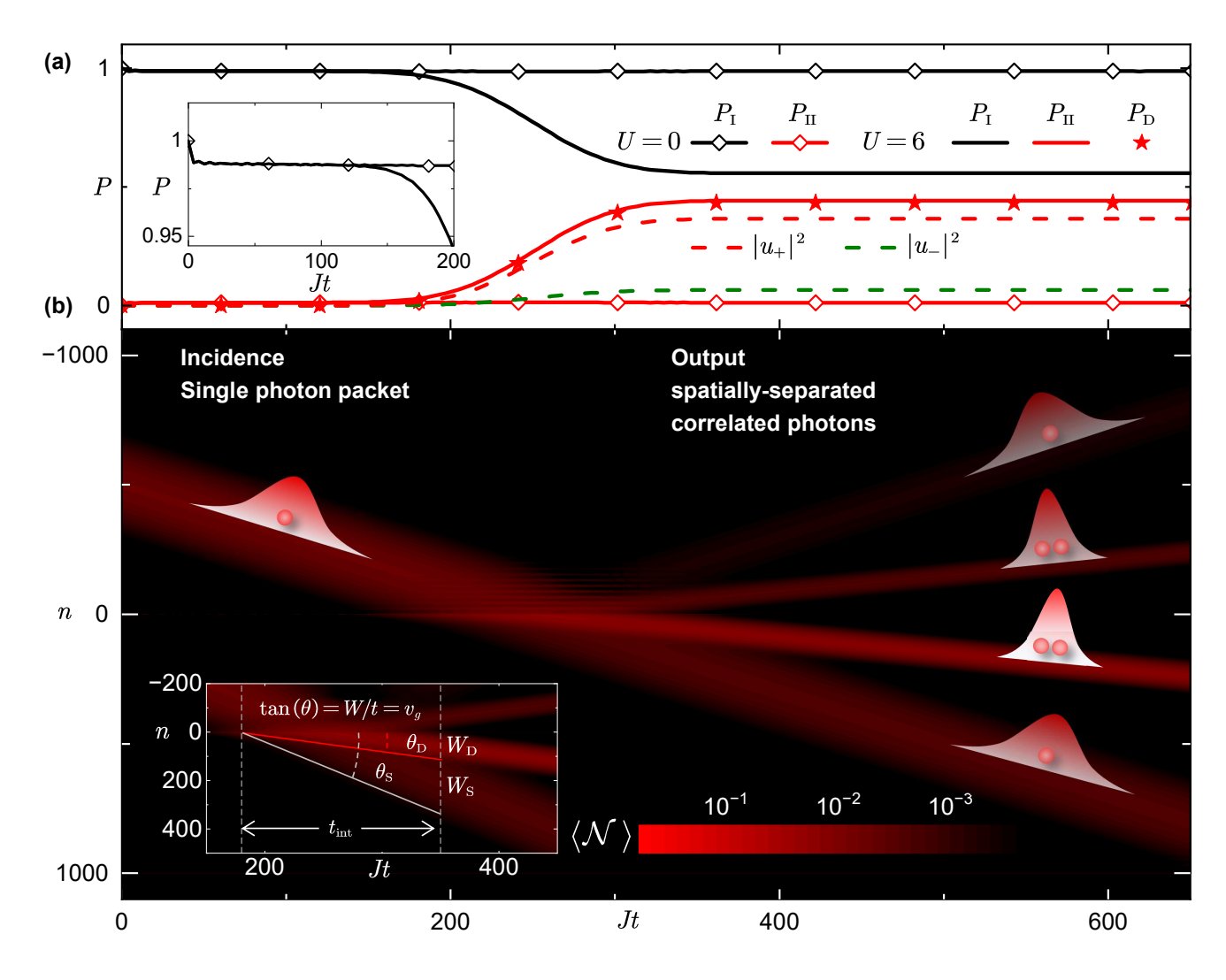


FIG. 5. Scattering into spatially separated correlated photons. (a) Time evolution of the populations, including the single-photon state $P_{\rm I}$, the full two-photon state $P_{\rm II}$, the doublon state $P_{\rm D}$, and the right-/left-going doublon components $|u_{\pm}|^2$, for different nonlinear strengths U=0 and U=6J. The inset shows the initial bound state population. (b) Photon number $\langle \mathcal{N} \rangle$ as a function of position n and time Jt. Following scattering, the incident photon splits into four distinct components: transmitted (t) and reflected (r) single photons, and right- and left-going doublon states u_{\pm} . The inset displays the natural spatial separation between single-photon and doublon states, arising from their distinct group velocities v_{k_0} and v_{K_r} , respectively. The coupling strength is here set to g=0.5J; all other parameters are the same as in Fig. 3.

at position n combines with the photon emitted from coupling point τ at position n_{τ} , incorporating the local phase ϕ_{τ} , to jointly excite a doublon in mode K. This excitation is characterized by an effective coupling strength $g_{|n-n_{\tau}|}$ and an accumulated propagation phase $\Phi_d = -K(n+n_{\tau})/2$, which depends on the center of mass of the two photons [39]. Note that Eq. (53) can be readily extended to the case of N coupling points, where $\tau = 1, 2, \ldots, N$.

Comparing Eq. (53) with the small-atom case in Eq. (16), we note that, using the PGA picture, pseudo-coupling points now form around each coupling point, with additional local phases $\phi_{l/r}$, as shown in Fig. 7(b). These pseudo-coupling points, associated with the coupling positions n_l and n_r , introduce new interference

pathways for doublon generation. When a single photon is located at n, the doublon can be generated via either the left (l) or right (r) coupling, corresponding to two distinct channels. In contrast to the case of a small emitter, where a single dominant channel prevails $(g_{n=0}\gg g_{n\neq 0})$, here both channels exhibit comparable strengths: $g_{|n_r-n_{\tau=r}|}=g_{|n_l-n_{\tau=l}|}=g$. Note that the coupling strength for each coupling point in Eq. (53) is initially uniform, but can be individually tuned by setting different values for g_l and g_r , enabling enhanced modulation flexibility. In this scenario, it is possible to engineer the multipoint coupling to realize higher conversion efficiency and optimal interference condition to achieve $u_+\gg u_-\simeq 0$, enabling the unidirectional generation of a doublon.

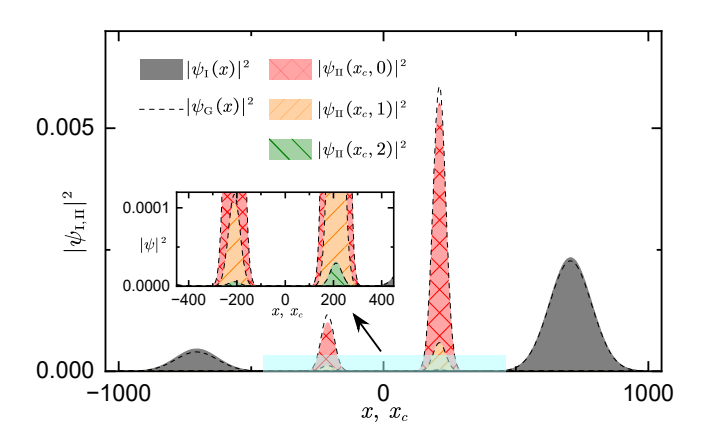


FIG. 6. Spatial distribution of the single-photon field $|\psi_{\rm I}(x)|^2$ and the two-photon field $|\psi_{\rm II}(x_c,r)|^2$ at Jt=600 from Fig. 5. Black solid curves represent analytical Gaussian wave packets [Eq. (49)], with spectral width L_G for the single photons and $L_G v_{K_r}/v_{k_0}$ for the doublons. Amplitudes are $|t|^2$, $|r|^2$ and $|u_{\pm}|^2 \times u(r)$ for the different components of the photon field.

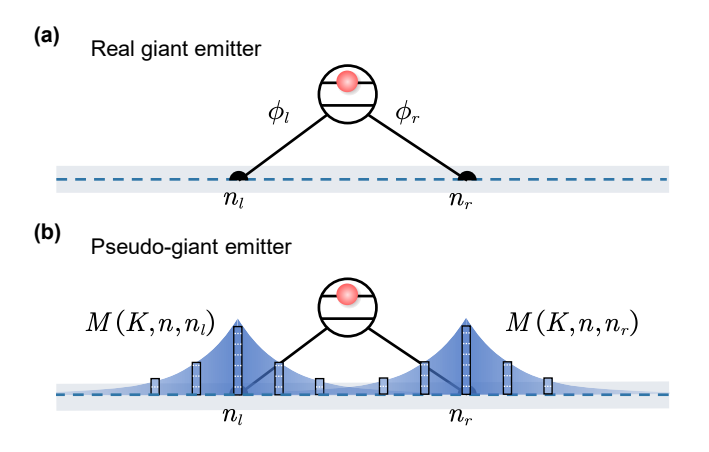


FIG. 7. Layout with an RGA. (a) The emitter couples to the waveguide at two points $n_{l/r}$ with encoded local phase $\phi_{l/r}$, forming an RGA. (b) In the PGA picture, sets of pseudocoupling points form around the coupling positions n_l and n_r .

By extending the derivation of the Lippmann-Schwinger equations to the giant-emitter interaction Hamiltonian in Eq. (53), we identify an optimal interference regime in which the emitter couples to the waveguide at three points $\{-1,0,1\}$ with equal coupling strengths $\{g,g,g\}$ and encoded phases $\{-\phi,0,+\phi\}$. In this configuration, Fig. 8(a) shows the population of key physical quantities as functions of g and ϕ . At the parameter values indicated by the white arrow, the conversion efficiency approaches unity, signifying complete conversion of the incident single photon into a doublon state, accompanied by full emitter relaxation and vanishing single-photon transmission and reflection. Theoretically, the doublon field exhibits unidirectional propagation, with $|u_{+K_r}|^2 \simeq 1$ and $|u_{-K_r}|^2 \simeq 0$, indicating optimal chirality in the output. Both the conversion efficiency and the

chiral factor can be smoothly tuned across the full range (0,1) by varying the coupling parameters g and ϕ .

Figure 8(b) compares numerical simulation results with the analytical solution, using the parameters indicated by the white dashed lines in Fig. 8(a). The analytical predictions match the numerical data well. Using the optimal coupling parameters identified in Fig. 8, we simulate the time evolution of the photonic field, as shown in Fig. 9. The incident single photon is unidirectionally converted into a doublon, akin to optical refraction into a slow-light mode with a low group velocity. The simulated conversion efficiency reaches 94%, with negligible single-photon transmission and reflection. The mismatch with the theoretical results is caused by the initial bound state, as shown by the gray solid curve in Fig. 8(b). In Appendix B, when a Lorentzian wavepacket is incident instead, we achieve conversion efficiency identical to the Gaussian case. Moreover, by tuning the coupling parameters, the scattering dynamics can be fully controlled, enabling continuous modulation of the conversion efficiency and backscattering-free, cascaded correlated photon-pair generation.

V. CASCADED SCATTERING PROCESS: GENERATING SPATIALLY SEPARATED CORRELATED N-PHOTON STATES

In the Bose–Hubbard model, higher-order multiphoton bound states beyond the doublon are also present [14]. As the photon number in these correlated states increase, the interaction-induced energy shift becomes larger, and the effective mass grows accordingly. By leveraging the mediation role of the emitter, the generated doublon can further scatter into a three-photon bound state, a triplon, which in turn may scatter into even higher-order states, enabling a cascaded nonlinear scattering process. Moreover, each successive bound state exhibits a heavier effective mass and a slower group velocity. This velocity hierarchy leads to natural spatial separation among the different photon-number components after propagation. The resulting state is a spatiotemporally structured multiphoton entangled state, with distinct groups of photons propagating at different speeds and localized in different regions of space.

A. Triplon generation

In this section, we further investigate a doublon wave packet scattering off a second excited emitter, leading to the formation of a three-photon bound state, a triplon, as shown in Fig. 1(a). The triplon band lies below the doublon bands, with a larger energy shift of 3U from the single-photon band. We consider the energy configuration illustrated in Fig. 1, where the frequency of the second emitter Δ_{e2} satisfies the resonance condition $E_{\mathcal{K}_r} = \Delta_{e2} + E_{K_r}$, with $E_{\mathcal{K}}$ denoting the triplon disper-

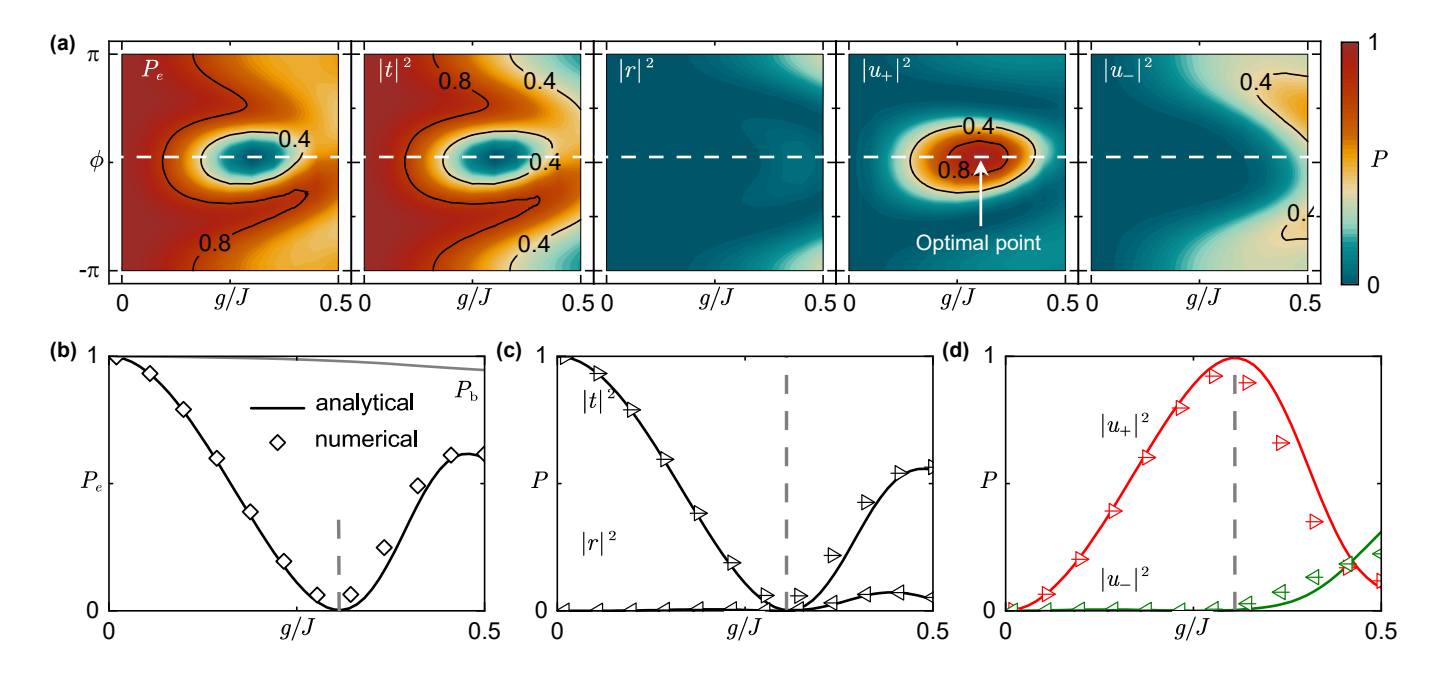


FIG. 8. Finding optimal parameters for conversion to doublons. (a) The physical quantities P_e , $|t|^2$, $|r|^2$, and $|u_{\pm}|^2$ as functions of coupling strength g and local phase ϕ , for a giant emitter with coupling strengths $\{g,g,g\}$ and coupling phases $\{-\phi,0,\phi\}$. (b–d) The lower panels show cross-section cuts along the white lines in the upper panels, comparing numerical simulations (diamond and triangular markers) with analytical solutions (solid curves). An optimal point exists at g=0.31J and $\phi=0.05\pi$, where the incident single photon is fully converted into a right-going doublon. This point is indicated by the white arrow in the upper panels and dashed vertical gray lines in the lower panels. All other parameters are the same as in Fig. 5.

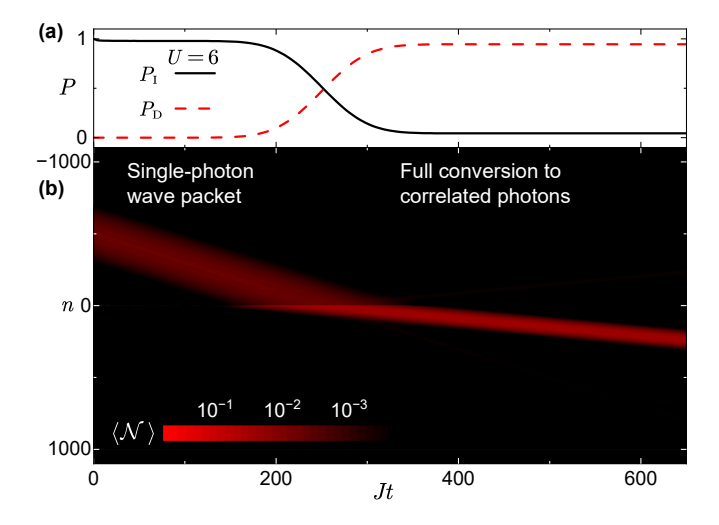


FIG. 9. Conversion to a doublon. (a) Populations of the single- and two-photon states. (b) Photon number $\langle \mathcal{N} \rangle$ as a function of position n and time Jt. Following scattering, the single photon is fully converted into a right-going doublon. Parameters correspond to the optimal operating point found in Fig. 8 $(g=0.31J,\,\phi=0.05\pi)$, and are otherwise the same as in Fig. 5.

sion relation and K the triplon momentum. The second emitter couples to the waveguide at n_2 with coupling strength g_2 .

Following the derivation in the previous section, the

interaction Hamiltonian for the triplon generation can be written as

$$H_{\rm int} = g_2 \sum_{\mathcal{K}, K} M^*(\mathcal{K}, K, n_2) T_{\mathcal{K}}^{\dagger} D_K \sigma_-, \tag{54}$$

where $T_{\mathcal{K}}^{\dagger}$ is the creation operator for the triplon state \mathcal{K} . The transition-matrix element is $M(\mathcal{K},K,n_2)=\langle \mathrm{vac}|D_Ka_{n_2}T_{\mathcal{K}}^{\dagger}|\mathrm{vac}\rangle$, between the incoming state $|K,n_2\rangle$ and the outgoing triplon state $|\mathcal{K}\rangle$. The transition rate is proportional to the overlap between two three-photon states: one is the correlated three-photon state; the other consists of a doublon state K and a single photon located at n_2 emitted by the second emitter. During the scattering process where the doublon is converted into a triplon, the localized coupling of emitter 2 behaves as a PGA, due to the spatial extent of the triplon wave function.

In Fig. 10, we present numerical simulations of this second scattering stage, building upon the initial state generated in the first stage (see Fig. 9). To enhance the triplon conversion efficiency, the second emitter is implemented as an RGA, coupling to the waveguide at three points $\{n_2-1,n_2,n_2+1\}$ with equal coupling strength and phase configuration $\{\phi,0,\phi\}$. By jointly optimizing the coupling parameters of both giant emitters, we achieve a nearly complete cascade: an incident single photon (S) is first converted into a two-photon bound state (doublon D), which is subsequently converted into a three-photon bound state (triplon T), as shown in Fig. 10(a) and Fig. 10(b). This stepwise energy trans-

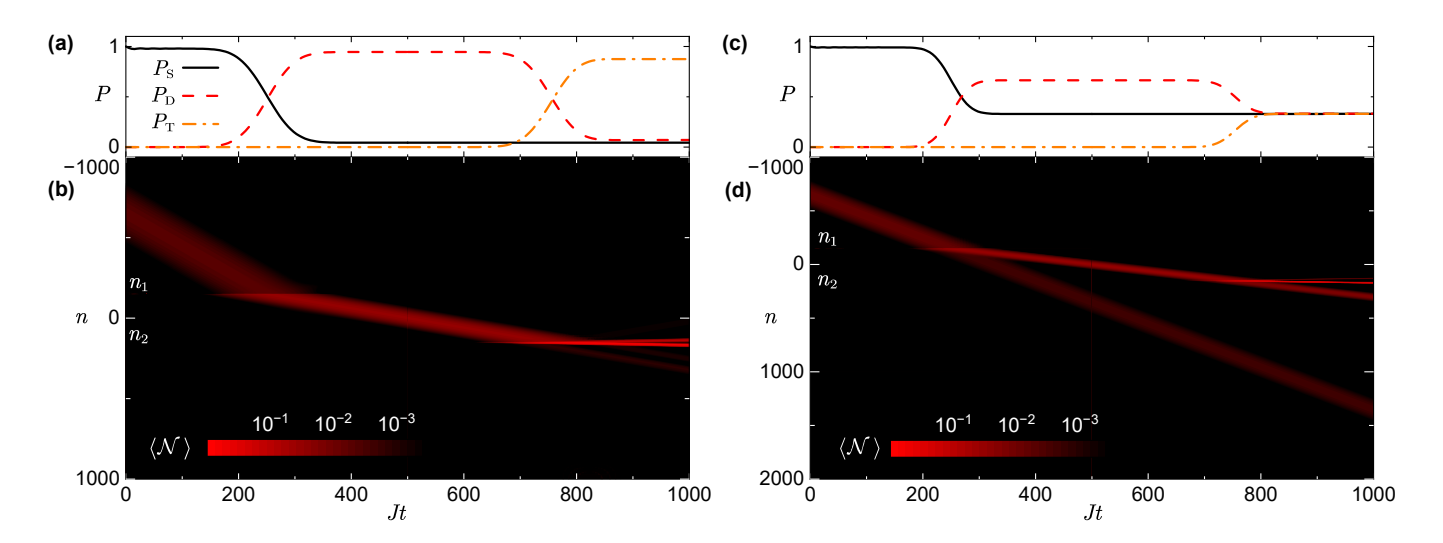


FIG. 10. Cascaded scattering process in a nonlinear waveguide. (a, c) Populations of the single-photon, doublon, and triplon states. (b, d) Photon number $\langle \mathcal{N} \rangle$ as a function of position x and time Jt. The frequency of the second emitter is $\Delta_{e2} = -11.869J$. Emitter positions are fixed at $n_1 = -150$ and $n_2 = 150$. Parameters for (a, b): $g_1 = 0.31J$, $\phi_1 = 0.05\pi$, $g_2 = 0.042J$, $\phi_2 = 0.167\pi$, and $L_G = 0.002$. Parameters for (c,d): $g_1 = 0.202J$, $\phi_1 = 0.05\pi$, $g_2 = 0.0255J$, $\phi_2 = 0$ and $L_G = 0.003$. All other parameters are the same as in Fig. 9.

fer across multiple quantum nonlinear stages resembles optical refraction across a series of media, with each mediating a mode conversion.

Moreover, the conversion efficiency for doublons and triplons can be continuously tuned by adjusting the coupling parameters of the giant-atom setup. In Fig. 10(c) and Fig. 10(d), we observe an approximately equal partition of the photon population among the single-, two-, and three-photon subspaces. As the photon number increases, the effective mass of the bound state grows and its group velocity decreases accordingly. At late times, the three wave-packet components (the single-photon, doublon, and triplon states) are naturally separated in space.

Note that the energy $\omega_{k_0} + \Delta_{e2}$ does not resonate with any eigenmode of the nonlinear waveguide. Consequently, the second emitter cannot couple the incident single photon to any photonic excitation. Although part of the single photon transmits through the first emitter, it propagates freely past the second emitter without significant scattering. In contrast, the second emitter and the incoming doublon state satisfy the resonance condition $E_{\mathcal{K}_r} = \Delta_{e2} + E_{K_r}$. This selective interaction mechanism enables the emitter to act as a "scattering trigger", activated only upon arrival of a correlated two-photon state.

By harnessing multi-photon bound states in the nonlinear waveguide and the engineered coupling of RGAs, the system realizes a deterministic cascaded scattering process, $S \to D \to T$. Given the existence of higher-order bound states in such systems, this sequential nonlinear conversion can, in principle, be extended to generate increasingly complex correlated photonic states through sequential nonlinear conversion. This architecture enables the deterministic encoding of quantum information into

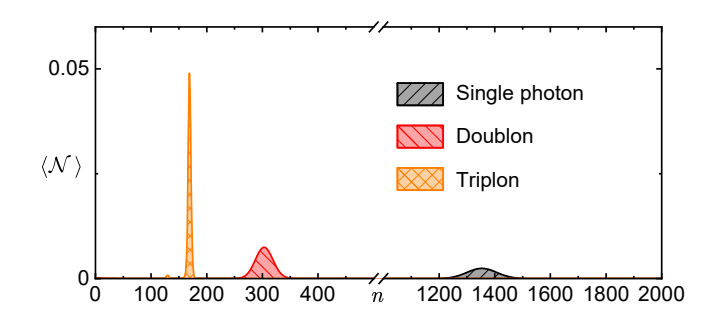


FIG. 11. Output spatiotemporal entanglement of the photonic field at Jt=1000 from Fig. 10(d). The single-photon, doublon, and triplon wave packets are spatially separated due to their photon-number-dependent group velocities, forming a multipartite quantum state with entanglement between arrival time and photon number.

propagating multiphoton states, "flying qubits", with enhanced correlation depth, paving the way toward scalable generation of entangled photonic clusters.

B. Spatial and temporal entanglement

The cascaded scattering process culminates in a spatiotemporally ordered quantum superposition, where the incident single photon, doublon, and triplon automatically separate into distinct space-time bins due to their photon-number-dependent group velocities. As derived analytically and visualized in Fig. 11, the final state evolves into

$$|\Psi_{\text{out}}\rangle \simeq \alpha |S\rangle_{\tau_1} + \beta |D\rangle_{\tau_2} + \gamma |T\rangle_{\tau_3},$$
 (55)

where

$$|S\rangle \equiv a_k^{\dagger} |\text{vac}, e, e\rangle,$$
 (56)

$$|D\rangle \equiv D_K^{\dagger} |\text{vac}, g, e\rangle,$$
 (57)

$$|T\rangle \equiv T_K^{\dagger} |\text{vac}, g, g\rangle,$$
 (58)

represent the single-photon, doublon, and triplon wave packet states, respectively. Here, the temporal ordering $\tau_1 < \tau_2 < \tau_3$ arises from the hierarchy of group velocities $v_g^{(1)} > v_g^{(2)} > v_g^{(3)}$, where the superscripts denote the photon number in each bound state. The spatial distribution of the doublon and triplon, characterized by center-of-mass coordinates x_c and X_c , allow their interpretation as composite bosonic quasiparticles. Additionally, the giant-atom coupling architecture enables flexible control of the superposition amplitudes $\alpha, \beta,$ and $\gamma,$ allowing programmable control of the output state.

This automatic spatiotemporal sorting transcends conventional time-bin entanglement schemes, which typically rely on time-dependent modulation pulses, multilevel emitters [61–67], or structured multimode baths [68]. In contrast, our architecture harnesses strongly correlated multi-photon bound states as intrinsic carriers of quantum information, enabling "correlated multi-photon flying qubits" with enhanced encoding capacity. The intrinsic non-classicality of the output state manifests through three distinct yet interrelated features:

- Photon-number superposition across temporal modes: The state exhibits a coherent superposition of different photon numbers in distinct spacetime bins, reflecting the temporal delocalization of quantum excitations.
- 2. Multi-photon bunching within bound-state wavepackets: Each localized wavepacket contains a well-defined multiphoton bound state, exhibiting strong internal photon-photon correlations, evidenced by bunching in the relative coordinates, within a single temporal mode.
- 3. Entanglement between arrival time and photon number: The final state is non-separable in the temporal and photonic number degrees of freedom, realizing entanglement between *when* the excitation arrives and *how many* photons it contains.

Harnessing the innate correlations in the spatial, temporal, and photon-number dimensions of the output states, this hybrid encoding scheme can multiplex them into a powerful framework for high-dimensional quantum information processing.

VI. CONCLUSION

We have established a paradigm for generating propagating multi-photon entangled states through cascaded

inelastic scattering in a nonlinear waveguide. The central point of this work is the discovery that a far detuned TLE can mediate photon-number upconversion $(S \to D \to T)$, bypassing the limitation of resonant scattering. This process is governed by an emergent nonlocal scattering potential, theoretically captured by the pseudo-giant atom formalism that we introduced, which reveals how the nonlinear multi-photon state reshapes the light–matter interaction.

By implementing this architecture with real giant atoms, we demonstrated unidirectional, high-efficiency conversion and programmable state synthesis, culminating in a self-sorted superposition of spatially and temporally isolated photon-number states. The resulting spatiotemporally entangled multi-photon state opens immediate pathways toward quantum-enhanced metrology through deterministic NOON-state synthesis [40, 69], distributed quantum computing using time-bin-encoded multi-photon graph states [70], and quantum state engineering via natural photon-number redistribution. More broadly, it bridges the gap between quantum nonlinear optics and correlated many-body physics, offering a scalable platform to explore exotic photonic matter.

This proposal is readily implementable in state-of-the-art superconducting circuits. An array of capacitively coupled transmons, whose intrinsic anharmonicity naturally provides the required nonlinear potential [19], can serve as the nonlinear waveguide considered in this work [21, 71]. Giant-atom architectures in superconducting circuits featuring multiple connection points, have already been experimentally demonstrated [32, 60]. Our results encourage further investigation of similar phenomena in nonlinear continuous waveguides and pave the way for future studies of nonlinear dynamics in various systems with photon-photon interactions.

ACKNOWLEDGMENTS

We are grateful to Dr. Tao Shi for useful discussions about scattering theory. The quantum dynamical simulations were performed using the open-source tools QuTiP [72–74] and QuSpin [75, 76]. X.W. is supported by the National Natural Science Foundation of China (NSFC) (Grant No. 12174303). A.F.K. acknowledges support from the Swedish Foundation for Strategic Research (grant numbers FFL21-0279 and FUS21-0063), the Horizon Europe programme HORIZON-CL4-2022-QUANTUM-01-SGA via the project 101113946 OpenSuperQPlus100, and from the Knut and Alice Wallenberg Foundation through the Wallenberg Centre for Quantum Technology (WACQT).

Appendix A: Derivations in momentum space

In this section, we derive the scattering state in momentum space, which is formally equivalent to the realspace treatment presented in Sec. IIIB. Applying a Fourier transform to convert the photon position coordinate x into the wave vector k, the interaction Hamiltonian is

$$H_{\text{int}} = \sum_{K} \sum_{k} g M^*(K, k, 0) D_K^{\dagger} \sigma_{-} a_k + \text{H.c.},$$
 (A1)

$$M(K, k, 0) = \frac{\sqrt{2}}{N} \sum_{m} e^{-ikm} e^{iKm/2} u_0 e^{-|m|/L_u(K)}, \quad (A2)$$

and the scattering-state solution has the form

$$|\Psi(t)\rangle = \left[\sum_{k} c_{e,k}(t)\sigma_{+}a_{k}^{\dagger} + \sum_{K} c_{K}(t)D_{K}^{\dagger}\right]|\text{vac}\rangle, \quad (A3)$$

where $c_{e,k}(t)$ denotes both the emitter and the singlephoton state k being excited. For notational simplicity, we suppress the emitter label, so that $c_{e,k} \to c_k$.

From the secular equation, we obtain the following system of equations:

$$(\omega_k + \Delta_e)c_k + g\sum_K M(K, k, n_0)c_K = (\omega_{k_0} + \Delta_e)c_k,$$
(A4)

$$E_K c_K + g \sum_k M^*(K, k, n_0) c_k = (\omega_{k_0} + \Delta_e) c_K.$$
 (A5)

Note that these equations describe the coupling between two momentum modes k and K. They can be rearranged into the form

$$c_k = \delta_{k,k_0} + g \sum_K \frac{M(K, k, n_0)c_K}{\omega_{k_0} - \omega_k + i0^+},$$
 (A6)

$$c_K = \frac{g \sum_k M^*(K, k, n_0) c_k}{E_K - E_K + i0^+},$$
(A7)

where δ_{k,k_0} indicates that the initial state is a right-going single photon.

By defining [49]

$$C_0(m) = \sum_k e^{ikm} c_k, \tag{A8}$$

we obtain a complex convolution equation

$$C_0(m_0) = e^{ik_0 m_0} - \frac{1}{v_{k_0} v_{K_r}} \times \sum_{m_1, m_2} g_{m_1} g_{m_2} e^{iK_r |m_1 - m_2|/2} e^{ik_0 |m_0 - m_1|} C_0(m_2), \quad (A9)$$

where

$$g_m = \sqrt{2}u_0 g e^{-|m|/L_u(K_r)}$$
 (A10)

denotes the effective coupling strength per pseudocoupling point of the PGA. The first term in Eq. (A9), $\exp(ik_0m_0)$, corresponds to the free propagation of the incident wave, while the second term captures the scatting disturbance due to the nonlocal potential. The convolution arises naturally from this nonlocality: the output $C_0(m_0)$ depends not only on the input at position m_0 , but also on the responses $C_0(m_2)$ at neighboring sites. This formulation describes multiple scattering events and reflects interference among different scattering channels.

Following the approach in Sec. III B, we find that the final state takes the form

$$|f_{i}\rangle = |\Psi(t \to \infty)\rangle \simeq \left[\sum_{\pm k} c_{e,\pm k}(+\infty)\sigma_{+}a_{\pm k}^{\dagger} + \sum_{\pm K} u_{\pm K}(+\infty)D_{\pm K}^{\dagger}\right]|\operatorname{vac}\rangle,$$
(A11)

where the momentum components are explicitly separated into positive and negative branches to distinguish the right- and left-going single-photon waves and the generation of doublon waves. After obtaining the scattering state for a single-photon plane-wave input, we now return to Eq. (18) to derive the output state by projecting the final state onto the subspaces spanned by $|e,k\rangle$ and $|K\rangle$, respectively.

1. Doublon component

We substitute the scattering state from Eq. (A3) and the interaction Hamiltonian from Eq. (A1) into Eq. (18), and project onto the right-going doublon state $|+K\rangle$, yielding

$$\langle +K|f\rangle = \langle +K|\Psi_{\rm sc}\rangle - \langle +K|\frac{1}{E_{K_r} - H_0 - i0^+}H_{\rm int}|\Psi_{\rm sc}\rangle$$

$$= \sum_{K'} \langle +K|\frac{g\sum_k M^*(K', k, n_0)c_k}{E_{K_r} - E_{K'} + i0^+}|K'\rangle$$

$$- \sum_{K'} \langle +K|\frac{g\sum_k M^*(K', k, n_0)c_k}{E_{K_r} - E_{K'} - i0^+}|K'\rangle. \quad (A12)$$

Using the expression for M in Eq. (A2), the definition of $C_0(m)$ in Eq. (A8), and evaluating the integrals via the retarded and advanced Green's functions Eqs. (34) and (35), we simplify Eq. (A12) to

$$\langle +K|f\rangle = \langle +K_r|f\rangle$$

$$= -i\frac{1}{v_{K_r}} \sum_{m} g_m e^{-iK_r m/2} [\Theta(-m) + \Theta(+m)] C_0(m)$$

$$= -i\frac{1}{v_{K_r}} \sum_{m} g_m e^{-iK_r m/2} C_0(m). \tag{A13}$$

Here, the retarded and advanced Green's functions, corresponding to the first and second terms in Eq. (A12), contribute $\Theta(-m)$ and $\Theta(+m)$, respectively. This temporal and spatial structure reflects the full scattering history: the initial state evolves into the scattering state under the retarded Green's function from $t=-\infty$ to

t=0, covering the negative spatial part of the nonlocal potential. The final state evolves back under the advanced Green's function from $t=+\infty$ to t=0, accounting for the positive spatial part. Together, these contributions encode the complete scattering process across both time $(t=-\infty \to t=0 \to t=+\infty)$ and space $(x=-\infty \to x=0 \to x=+\infty)$, as captured by the combination $\Theta(-x)+\Theta(+x)$. Thus, the doublon components of the final state are

$$u_{+K_r} = \langle +K_r | f \rangle = -i \frac{1}{v_{K_r}} \sum_m g_m e^{-iK_r m/2} C_0(m),$$

$$(A14)$$

$$u_{-K_r} = \langle -K_r | f \rangle = -i \frac{1}{v_{K_r}} \sum_m g_m e^{+iK_r m/2} C_0(m).$$

$$(A15)$$

2. Single-photon component

We now project the final state onto the right-going single-photon state $|+k,e\rangle$ (suppressing the emitter label, we denote this state as $|k\rangle$):

$$\langle +k|f\rangle = \langle +k|\Psi_{\rm sc}\rangle - \langle +k|\frac{1}{E - H_0 - i0^+}H_{\rm int}|\Psi_{\rm sc}\rangle$$

$$= \langle +k| + k_0\rangle + \sum_k \langle +k|\frac{g\sum_K M(K, k, n_0)c_K}{\omega_{k_0} - \omega_k + i0^+}|k\rangle$$

$$-\sum_k \langle +k|\frac{g\sum_K M(K, k, n_0)c_K}{\omega_{k_0} - \omega_k - i0^+}|k\rangle. \tag{A16}$$

Here, the first term corresponds to the initial state [i.e., the δ_{k,k_0} in Eq. (A6)].

The Green's function integrals over k are

$$\frac{1}{N} \sum_{k} \frac{e^{-ikm/2}}{\omega_{k_0} - \omega_k + i0^+} |k\rangle = -\frac{i}{v_k} \times \left[e^{-ik_0m/2} \Theta(-m) |+k_0\rangle + e^{ik_0m/2} \Theta(+m) |-k_0\rangle \right], \text{ (A17)}$$

$$\frac{1}{N} \sum_{k} \frac{e^{-ikm/2}}{\omega_{k_0} - \omega_k - i0^+} |k\rangle = +i \frac{1}{v_k} \times \left[e^{-ik_0m/2} \Theta(+m) |+k_0\rangle + e^{ik_0m/2} \Theta(-m) |-k_0\rangle \right]. \text{ (A18)}$$

Thus, Eq. (A16) is

$$\langle +k_0|f\rangle = 1 + \sum_{m_1} \frac{-i}{v_k} g_{m_1} e^{-ik_0 m_1} \sum_K e^{iKm_1/2} c_K.$$
 (A19)

The summation over K can be evaluated using Eq. (A7):

$$\sum_{K} e^{iKm_1/2} c_K = \sum_{m_2} \frac{-i}{v_{K_r}} e^{iK_r |m_1 - m_2|/2} g_{m_2} C_0(m_2).$$
(A20)

The final state amplitudes for the single-photon components are then

$$t = \langle +k_0, e|f \rangle = 1 - \frac{1}{v_{k_0} v_{K_r}} \sum_{m_1, m_2} g_{m_1} g_{m_2} e^{-ik_0 m_1} e^{iK_r |m_1 - m_2|/2} C_0(m_2),$$

$$(A21)$$

$$r = \langle -k_0, e|f \rangle = -\frac{1}{v_{k_0} v_{K_r}} \sum_{m_1, m_2} g_{m_1} g_{m_2} e^{ik_0 m_1} e^{iK_r |m_1 - m_2|/2} C_0(m_2).$$

$$(A22)$$

Ultimately, the final outgoing state, given an initial incident single-photon plane wave $\exp(ik_0x)$, is

$$|i\rangle = |e, +k_0\rangle, \tag{A23}$$

$$|f_i\rangle = t |e, +k_0\rangle + r |e, -k_0\rangle + u_{\pm K_r} |\pm K_r\rangle,$$
 (A24)

where t and r denote the transmission and reflection amplitudes, respectively, of the single photon, and $u_{\pm K_r}$ is the probability amplitudes for the generated right- and left-going doublon modes. Note that, although the incident state only consists of a single-photon plane wave, the scattered state contains not only the reflection r and transmission t single-photon components, but also the right- and left-going doublon waves $|\pm K_r\rangle$. The final results can be obtained numerically by solving the complex convolution equation [Eq. (A9)] for $C_0(m)$, and then substituting into Eqs. (A14), (A15), (A21), and (A22).

Appendix B: The wave-packet shape

In our analytical derivation, we assume the incident wave packet to be a plane wave, i.e., $|\psi(t=0)\rangle = \exp(ik_0x)$. For a specific single mode k, this assumption allows the computation of the corresponding scattering amplitudes, such as t(k), r(k), and $u_{\pm K_r}(k)$], each of which depends on k. Similar to the Wigner-Weisskopf approximation, if the momentum spread of the wave packet is much smaller than the single-photon bandwidth $(L_G \ll 4J)$, the dispersion near k_0 can be approximated as linear. In this regime, the narrow momentum distribution can be effectively treated as centered around k_0 . Consequently, the scattering amplitudes can be approximated as constants: $[t(k_0), r(k_0), u_{\pm K_r}(k_0)]$. This approximation is validated numerically in Fig. 3.

We also perform numerical simulations using a Lorentzian wave packet. The initial state in momentum and real space is then given by

$$\psi_{L}(k) = \sqrt{\frac{L_{L}}{\pi}} \frac{1}{L_{L} - i(k - k_{0})},$$

$$\psi_{L}(x) = \sqrt{2L_{L}} e^{ik_{0}x} e^{xL_{L}} \Theta(-x_{0}).$$
(B1)

Here, $L_{\rm L}$ denotes the spatial spread of the Lorentzian wave packet. Using the same simulation parameters as

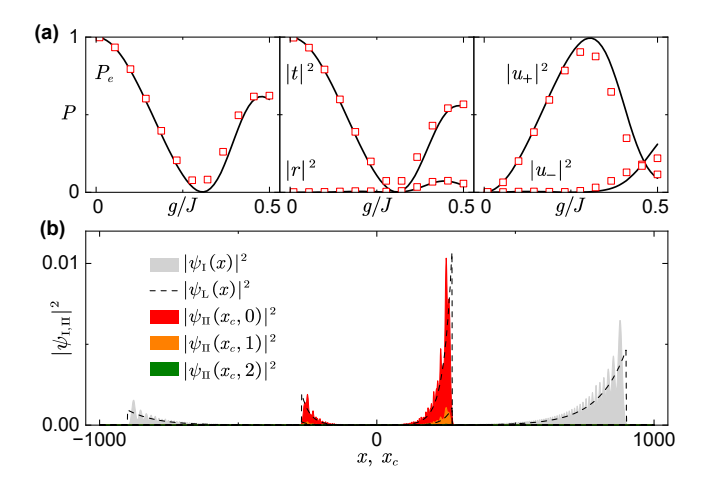


FIG. 12. Scattering results for a Lorentzian wave packet. (a) The physical quantities as a function of g with the initial Lorentzian wave packet shape from Eq. (B1). (b) The scattering field. The parameters are the same as in Fig. 8 in the main text.

for the Gaussian wave packet discussed in the main text, we present the results in Fig. 12. After scattering, the generated doublon wave retains the profile of the incident photon wave packet, albeit with a modified bandwidth $W_D = (v_K/v_k)W_S$.

- S. L. Rolston and W. D. Phillips, Nonlinear and quantum atom optics, Nature 416, 219 (2002).
- [2] D. E. Chang, V. Vuletic, and M. D. Lukin, Quantum nonlinear optics — photon by photon, Nat. Photon. 8, 685 (2014).
- [3] J. Bloch, A. Cavalleri, V. Galitski, M. Hafezi, and A. Rubio, Strongly correlated electron-photon systems, Nature 606, 41 (2022).
- [4] D. Roy, C. M. Wilson, and O. Firstenberg, Colloquium: Strongly interacting photons in one-dimensional continuum, Rev. Mod. Phys. 89, 021001 (2017).
- [5] D. E. Chang, J. S. Douglas, A. González-Tudela, C.-L. Hung, and H. J. Kimble, Colloquium: Quantum matter built from nanoscopic lattices of atoms and photons, Rev. Mod. Phys. 90, 031002 (2018).
- [6] A. S. Sheremet, M. I. Petrov, I. V. Iorsh, A. V. Poshakinskiy, and A. N. Poddubny, Waveguide quantum electrodynamics: Collective radiance and photon-photon correlations, Rev. Mod. Phys. 95, 015002 (2023).
- [7] A. Gonzalez-Tudela, A. Reiserer, J. J. Garcia-Ripoll, and F. J. Garcia-Vidal, Light-matter interactions in quantum nanophotonic devices, Nat. Rev. Phys. 6, 166 (2024).
- [8] A. S. Prasad, J. Hinney, S. Mahmoodian, K. Hammerer, S. Rind, P. Schneeweiss, A. S. Sørensen, J. Volz, and A. Rauschenbeutel, Correlating photons using the collective nonlinear response of atoms weakly coupled to an optical mode, Nat. Photon, 14, 719 (2020).
- [9] A. V. Poshakinskiy, J. Zhong, Y. Ke, N. A. Olekhno, C. Lee, Y. S. Kivshar, and A. N. Poddubny, Quantum Hall phases emerging from atom-photon interactions, npj Quantum Inf. 7, 34 (2021).
- [10] G. Calajo and D. E. Chang, Emergence of solitons from many-body photon bound states in quantum nonlinear media, Phys. Rev. Res. 4, 023026 (2022).
- [11] T. Peyronel, O. Firstenberg, Q.-Y. Liang, S. Hofferberth, A. V. Gorshkov, T. Pohl, M. D. Lukin, and V. Vuletić, Quantum nonlinear optics with single photons enabled

- by strongly interacting atoms, Nature 488, 57 (2012).
- [12] P. Lodahl, S. Mahmoodian, and S. Stobbe, Interfacing single photons and single quantum dots with photonic nanostructures, Rev. Mod. Phys. 87, 347 (2015).
- [13] H. Le Jeannic, A. Tiranov, J. Carolan, T. Ramos, Y. Wang, M. H. Appel, S. Scholz, A. D. Wieck, A. Ludwig, N. Rotenberg, L. Midolo, J. J. Garcia-Ripoll, A. S. Sørensen, and P. Lodahl, Dynamical photon-photon interaction mediated by a quantum emitter, Nat. Phys. 18, 1191 (2022).
- [14] O. Mansikkamäki, S. Laine, A. Piltonen, and M. Silveri, Beyond Hard-Core Bosons in Transmon Arrays, PRX Quantum 3, 040314 (2022).
- [15] F. Schäfer, T. Fukuhara, S. Sugawa, Y. Takasu, and Y. Takahashi, Tools for quantum simulation with ultracold atoms in optical lattices, Nat. Rev. Phys. 2, 411 (2020).
- [16] J. Koch, T. M. Yu, J. Gambetta, A. A. Houck, D. I. Schuster, J. Majer, A. Blais, M. H. Devoret, S. M. Girvin, and R. J. Schoelkopf, Charge-insensitive qubit design derived from the Cooper pair box, Phys. Rev. A 76, 042319 (2007).
- [17] X. Gu, A. F. Kockum, A. Miranowicz, Y.-X. Liu, and F. Nori, Microwave photonics with superconducting quantum circuits, Phys. Rep. 718-719, 1 (2017).
- [18] T. Orell, A. A. Michailidis, M. Serbyn, and M. Silveri, Probing the many-body localization phase transition with superconducting circuits, Phys. Rev. B 100, 134504 (2019).
- [19] A. Blais, A. L. Grimsmo, S. M. Girvin, and A. Wallraff, Circuit quantum electrodynamics, Rev. Mod. Phys. 93, 025005 (2021).
- [20] G. P. Fedorov, S. V. Remizov, D. S. Shapiro, W. V. Pogosov, E. Egorova, I. Tsitsilin, M. Andronik, A. A. Dobronosova, I. A. Rodionov, O. V. Astafiev, and A. V. Ustinov, Photon Transport in a Bose-Hubbard Chain of Superconducting Artificial Atoms, Phys. Rev. Lett. 126,

- 180503 (2021).
- [21] A. H. Karamlou, I. T. Rosen, S. E. Muschinske, C. N. Barrett, A. Di Paolo, L. Ding, P. M. Harrington, M. Hays, R. Das, D. K. Kim, B. M. Niedzielski, M. Schuldt, K. Serniak, M. E. Schwartz, J. L. Yoder, S. Gustavsson, Y. Yanay, J. A. Grover, and W. D. Oliver, Probing entanglement in a 2D hard-core Bose-Hubbard lattice, Nature 629, 561 (2024).
- [22] M. D. Lukin, M. Fleischhauer, R. Cote, L. M. Duan, D. Jaksch, J. I. Cirac, and P. Zoller, Dipole Blockade and Quantum Information Processing in Mesoscopic Atomic Ensembles, Phys. Rev. Lett. 87, 037901 (2001).
- [23] A. V. Gorshkov, J. Otterbach, M. Fleischhauer, T. Pohl, and M. D. Lukin, Photon-Photon Interactions via Rydberg Blockade, Phys. Rev. Lett. 107, 133602 (2011).
- [24] P. Weckesser, K. Srakaew, T. Blatz, D. Wei, D. Adler, S. Agrawal, A. Bohrdt, I. Bloch, and J. Zeiher, Realization of a Rydberg-dressed extended Bose Hubbard model (2024), arXiv:2405.20128.
- [25] R. Piil and K. Mølmer, Tunneling couplings in discrete lattices, single-particle band structure, and eigenstates of interacting atom pairs, Phys. Rev. A 76, 023607 (2007).
- [26] M. Valiente and D. Petrosyan, Two-particle states in the Hubbard model, J. Phys. B: At. Mol. Opt. Phys. 41, 161002 (2008).
- [27] M. Valiente, D. Petrosyan, and A. Saenz, Three-body bound states in a lattice, Phys. Rev. A 81, 011601 (2010).
- [28] A. F. Kockum, Quantum Optics with Giant Atoms—the First Five Years, in *International Symposium on Mathematics, Quantum Theory, and Cryptography (Mathematics for Industry, vol 33)* (Springer, 2021) pp. 125–146.
- [29] M. V. Gustafsson, T. Aref, A. F. Kockum, M. K. Ekström, G. Johansson, and P. Delsing, Propagating phonons coupled to an artificial atom, Science 346, 207 (2014).
- [30] A. Frisk Kockum, P. Delsing, and G. Johansson, Designing frequency-dependent relaxation rates and Lamb shifts for a giant artificial atom, Phys. Rev. A 90, 013837 (2014).
- [31] A. F. Kockum, G. Johansson, and F. Nori, Decoherence-Free Interaction between Giant Atoms in Waveguide Quantum Electrodynamics, Phys. Rev. Lett. 120, 140404 (2018).
- [32] B. Kannan, M. J. Ruckriegel, D. L. Campbell, A. Frisk Kockum, J. Braumüller, D. K. Kim, M. Kjaergaard, P. Krantz, A. Melville, B. M. Niedzielski, A. Vepsäläinen, R. Winik, J. L. Yoder, F. Nori, T. P. Orlando, S. Gustavsson, and W. D. Oliver, Waveguide quantum electrodynamics with superconducting artificial giant atoms, Nature 583, 775 (2020).
- [33] S. Mahmoodian, G. Calajo, D. E. Chang, K. Hammerer, and A. S. Sørensen, Dynamics of Many-Body Photon Bound States in Chiral Waveguide QED, Phys. Rev. X 10, 031011 (2020).
- [34] N. Tomm, S. Mahmoodian, N. O. Antoniadis, R. Schott, S. R. Valentin, A. D. Wieck, A. Ludwig, A. Javadi, and R. J. Warburton, Photon bound state dynamics from a single artificial atom, Nat. Phys. 19, 857 (2023).
- [35] J. J. Sakurai and J. Napolitano, Modern Quantum Mechanics (Cambridge University Press, 2017).
- [36] K. Winkler, G. Thalhammer, F. Lang, R. Grimm, J. Hecker Denschlag, A. J. Daley, A. Kantian, H. P. Büchler, and P. Zoller, Repulsively bound atom pairs in an optical lattice, Nature 441, 853 (2006).

- [37] J. S. Douglas, T. Caneva, and D. E. Chang, Photon Molecules in Atomic Gases Trapped Near Photonic Crystal Waveguides, Phys. Rev. X 6, 031017 (2016).
- [38] Z. Wang, T. Jaako, P. Kirton, and P. Rabl, Supercorrelated Radiance in Nonlinear Photonic Waveguides, Phys. Rev. Lett. 124, 213601 (2020).
- [39] X. Wang, J.-Q. Li, Z. Wang, A. F. Kockum, L. Du, T. Liu, and F. Nori, Nonlinear chiral quantum optics with giant-emitter pairs (2024), arXiv:2404.09829.
- [40] E. Compagno, L. Banchi, C. Gross, and S. Bose, NOON states via a quantum walk of bound particles, Phys. Rev. A 95, 012307 (2017).
- [41] T. Shi, Y.-H. Wu, A. González-Tudela, and J. I. Cirac, Bound States in Boson Impurity Models, Phys. Rev. X 6, 021027 (2016).
- [42] S. John and J. Wang, Quantum electrodynamics near a photonic band gap: Photon bound states and dressed atoms, Phys. Rev. Lett. 64, 2418 (1990).
- [43] A. Imamoğlu, H. Schmidt, G. Woods, and M. Deutsch, Strongly Interacting Photons in a Nonlinear Cavity, Phys. Rev. Lett. 79, 1467 (1997).
- [44] J.-Q. Li and X. Wang, Environmental Quantum States Trigger Emission in Nonlinear Photonics (2025), arXiv:2505.03640.
- [45] M. O. Scully and M. S. Zubairy, Quantum Optics (Cambridge University Press, 1997).
- [46] J.-T. Shen and S. Fan, Strongly correlated multiparticle transport in one dimension through a quantum impurity, Phys. Rev. A 76, 062709 (2007).
- [47] E. Rephaeli and S. Fan, Stimulated Emission from a Single Excited Atom in a Waveguide, Phys. Rev. Lett. 108, 143602 (2012).
- [48] E. Sanchez-Burillo, D. Zueco, J. J. Garcia-Ripoll, and L. Martin-Moreno, Scattering in the Ultrastrong Regime: Nonlinear Optics with One Photon, Phys. Rev. Lett. 113, 263604 (2014).
- [49] T. Shi, Y. Chang, and J. J. García-Ripoll, Ultrastrong Coupling Few-Photon Scattering Theory, Phys. Rev. Lett. 120, 153602 (2018).
- [50] X. Wang and H.-R. Li, Chiral quantum network with giant atoms, Quantum Sci. Technol. 7, 035007 (2022).
- [51] J. R. Taylor, Scattering theory: the quantum theory of nonrelativistic collisions (Courier Corporation, 2012).
- [52] J.-T. Shen and S. Fan, Theory of single-photon transport in a single-mode waveguide. I. Coupling to a cavity containing a two-level atom, Phys. Rev. A 79, 023837 (2009)
- [53] J.-T. Shen and S. Fan, Theory of single-photon transport in a single-mode waveguide. II. Coupling to a whisperinggallery resonator containing a two-level atom, Phys. Rev. A 79, 023838 (2009).
- [54] Z. Wang, L. Du, Y. Li, and Y.-x. Liu, Phase-controlled single-photon nonreciprocal transmission in a one-dimensional waveguide, Phys. Rev. A 100, 053809 (2019).
- [55] Y.-T. Chen, L. Du, L. Guo, Z. Wang, Y. Zhang, Y. Li, and J.-H. Wu, Nonreciprocal and chiral single-photon scattering for giant atoms, Commun. Phys. 5, 215 (2022).
- [56] Y. Xue and Y. xi Liu, Two-photon scattering in a waveguide by a giant atom (2025), arXiv:2501.14464.
- [57] L. Brillouin, Wave propagation and group velocity, Vol. 8 (Academic press, 2013).
- [58] A. Bers, Note on group velocity and energy propagation, Am. J. Phys 68, 482 (2000).

- [59] N. M. R. Peres, Scattering in one-dimensional heterostructures described by the Dirac equation, J. Phys.: Condens. Matter 21, 095501 (2009).
- [60] C. Joshi, F. Yang, and M. Mirhosseini, Resonance Fluorescence of a Chiral Artificial Atom, Phys. Rev. X 13, 021039 (2023).
- [61] K. M. Gheri, C. Saavedra, P. Törmä, J. I. Cirac, and P. Zoller, Entanglement engineering of one-photon wave packets using a single-atom source, Phys. Rev. A 58, R2627 (1998).
- [62] C. Schön, E. Solano, F. Verstraete, J. I. Cirac, and M. M. Wolf, Sequential Generation of Entangled Multiqubit States, Phys. Rev. Lett. 95, 110503 (2005).
- [63] H. Pichler, S. Choi, P. Zoller, and M. D. Lukin, Universal photonic quantum computation via time-delayed feedback, Proc. Natl. Acad. Sci. 114, 11362 (2017).
- [64] B. Kannan, D. L. Campbell, F. Vasconcelos, R. Winik, D. K. Kim, M. Kjaergaard, P. Krantz, A. Melville, B. M. Niedzielski, J. L. Yoder, T. P. Orlando, S. Gustavsson, and W. D. Oliver, Generating spatially entangled itinerant photons with waveguide quantum electrodynamics, Sci. Adv. 6, eabb8780 (2020).
- [65] J.-C. Besse, K. Reuer, M. C. Collodo, A. Wulff, L. Wernli, A. Copetudo, D. Malz, P. Magnard, A. Akin, M. Gabureac, G. J. Norris, J. I. Cirac, A. Wallraff, and C. Eichler, Realizing a deterministic source of multipartiteentangled photonic qubits, Nat. Commun. 11, 4877 (2020).
- [66] S. C. Wein, J. C. Loredo, M. Maffei, P. Hilaire, A. Harouri, N. Somaschi, A. Lemaitre, I. Sagnes, L. Lanco, O. Krebs, A. Auffeves, C. Simon, P. Senellart, and C. Antón-Solanas, Photon-number entanglement generated by sequential excitation of a two-level atom, Nat. Photon. 16, 374 (2022).
- [67] K. Tiurev, M. H. Appel, P. L. Mirambell, M. B. Lauritzen, A. Tiranov, P. Lodahl, and A. S. Sørensen, High-fidelity multiphoton-entangled cluster state with solid-state quantum emitters in photonic nanostructures,

- Phys. Rev. A 105, L030601 (2022).
- [68] C. Vega, D. Porras, and A. González-Tudela, Topological multimode waveguide QED, Phys. Rev. Res. 5, 023031 (2023).
- [69] S. Dengis, S. Wimberger, and P. Schlagheck, Multimode NOON-state generation with ultracold atoms via geodesic counterdiabatic driving, Phys. Rev. A 112, 042610 (2025).
- [70] G. F. Penas, J.-J. Garcia-Ripoll, and R. Puebla, Deterministic multipartite entanglement via fractional state transfer across quantum networks (2024), arXiv:2408.01177.
- [71] C. Castillo-Moreno, T. S'epulcre, T. Hillmann, K. R. Amin, M. Kervinen, and S. Gasparinetti, Experimental observation of multimode quantum phase transitions in a superconducting bose-hubbard simulator (2025), arXiv:2508.20116.
- [72] J. R. Johansson, P. D. Nation, and F. Nori, QuTiP: An open-source Python framework for the dynamics of open quantum systems, Comput. Phys. Commun. 183, 1760 (2012).
- [73] J. R. Johansson, P. D. Nation, and F. Nori, QuTiP 2: A Python framework for the dynamics of open quantum systems, Comput. Phys. Commun. 184, 1234 (2013).
- [74] N. Lambert, E. Giguère, P. Menczel, B. Li, P. Hopf, G. Suárez, M. Gali, J. Lishman, R. Gadhvi, R. Agarwal, A. Galicia, N. Shammah, P. Nation, J. R. Johansson, S. Ahmed, S. Cross, A. Pitchford, and F. Nori, QuTiP 5: The Quantum Toolbox in Python (2025), arXiv:2412.04705.
- [75] P. Weinberg and M. Bukov, QuSpin: a Python package for dynamics and exact diagonalisation of quantum many body systems part I: spin chains, SciPost Phys. 2, 003 (2017).
- [76] P. Weinberg and M. Bukov, QuSpin: a Python package for dynamics and exact diagonalisation of quantum many body systems. Part II: bosons, fermions and higher spins, SciPost Phys. 7, 020 (2019).